



**HAL**  
open science

## **A cardiac mitochondrial cAMP signaling pathway regulates calcium accumulation, permeability transition and cell death**

Zhenyu Wang, Dawei P. Liu, Audrey Varin, Valérie Nicolas, Delphine Courilleau, Philippe Mateo, Céline Caubère, Philippe Rouet, Ana-Maria Gomez, Grégoire Vandecasteele, et al.

### ► To cite this version:

Zhenyu Wang, Dawei P. Liu, Audrey Varin, Valérie Nicolas, Delphine Courilleau, et al.. A cardiac mitochondrial cAMP signaling pathway regulates calcium accumulation, permeability transition and cell death. *Cell Death and Disease*, 2016, 7 (4), pp.e2198-e2198. 10.1038/cddis.2016.106 . hal-02482657

**HAL Id: hal-02482657**

**<https://hal.science/hal-02482657>**

Submitted on 18 Feb 2020

**HAL** is a multi-disciplinary open access archive for the deposit and dissemination of scientific research documents, whether they are published or not. The documents may come from teaching and research institutions in France or abroad, or from public or private research centers.

L'archive ouverte pluridisciplinaire **HAL**, est destinée au dépôt et à la diffusion de documents scientifiques de niveau recherche, publiés ou non, émanant des établissements d'enseignement et de recherche français ou étrangers, des laboratoires publics ou privés.

# **A cardiac mitochondrial cAMP signaling pathway regulates calcium accumulation, permeability transition and cell death**

Zhenyu WANG<sup>1</sup>, Dawei Liu<sup>1</sup>, Audrey VARIN<sup>1</sup>, Valérie NICOLAS<sup>2</sup>, Delphine COURILLEAU<sup>2</sup>, Philippe MATEO<sup>1</sup>, Céline CAUBERE<sup>3</sup>, Philippe ROUET<sup>3</sup>, Ana-Maria GOMEZ<sup>1</sup>, Grégoire VANDECASTEELE<sup>1</sup>, Rodolphe FISCHMEISTER<sup>1,2</sup>, Catherine BRENNER<sup>1,2</sup>

<sup>1</sup> INSERM UMR-S 1180, Univ. Paris-Sud, Université Paris-Saclay, Châtenay-Malabry, France, <sup>2</sup> UMS-IPSIT, Univ. Paris-Sud, Université Paris-Saclay, Châtenay-Malabry, France; <sup>3</sup> INSERM I2MC, UMR 1048, Université Paul Sabatier, Toulouse, France

Short title: cardiac mitochondrial cAMP pathway

Correspondance to Dr Catherine Brenner  
INSERM UMR-S 1180  
Faculté de Pharmacie  
Université Paris-Sud  
5 Rue J.-B. Clément  
92296 Châtenay-Malabry Cedex  
France.  
E-mail: catherine.brenner-jan@u-psud.fr

**Abbreviations:** 2HE, 2-hydroxyestradiol; AC, adenylyl cyclase; ANT, adenine nucleotide translocase; CCCP, Carbonyl cyanide m-chlorophenyl hydrazone; CsA, cyclosporine A;  $\Delta\Psi_m$ , mitochondrial membrane potential; Epac, exchange protein directly activated by cAMP;  $\text{HCO}_3^-$ , bicarbonate; HF, heart failure; IM, inner membrane; MCU, mitochondrial calcium uniporter; mNCX, mitochondrial  $\text{Na}^+/\text{Ca}^{2+}$  exchanger; MPT, mitochondrial permeability transition; OM, outer membrane; PKA, protein kinase A; ROS, reactive oxygen species; sAC, soluble adenylyl cyclase; sAC<sub>fl</sub>, full-length soluble adenylyl cyclase; sAC<sub>t</sub>, truncated soluble adenylyl cyclase.

## Abstract

While cardiac cytosolic cAMP regulates multiple processes, such as beating, contractility, metabolism and apoptosis, little is known yet on the role of this second messenger within cardiac mitochondria. Using cellular and subcellular approaches, we demonstrate here the local expression of several actors of cAMP signaling within cardiac mitochondria, namely a truncated form of soluble AC (sAC<sub>t</sub>) and the exchange protein directly activated by cAMP 1 (Epac1) and show a protective role for sAC<sub>t</sub> against cell death, apoptosis as well as necrosis, in primary cardiomyocytes. Upon stimulation with bicarbonate (HCO<sub>3</sub><sup>-</sup>) and Ca<sup>2+</sup>, sAC<sub>t</sub> produces cAMP, which in turn stimulates oxygen consumption, increases the mitochondrial membrane potential ( $\Delta\Psi_m$ ) and ATP production. cAMP is rate-limiting for matrix Ca<sup>2+</sup> entry via the mitochondrial calcium uniporter (MCU) and, as a consequence, prevents mitochondrial permeability transition (MPT). The mitochondrial cAMP effects involve neither PKA, Epac2 nor the mitochondrial Na<sup>+</sup>/Ca<sup>2+</sup> exchanger (mNCX). In addition, in mitochondria isolated from failing rat hearts, stimulation of the mitochondrial cAMP pathway by HCO<sub>3</sub><sup>-</sup> rescued the sensitization of mitochondria to Ca<sup>2+</sup>-induced MPT. Thus, our study identifies a link between mitochondrial cAMP, mitochondrial metabolism and cell death in the heart, which is independent of cytosolic cAMP signaling. Our results might have implications for therapeutic prevention of cell death in cardiac pathologies.

**Keywords:** cAMP, calcium, mitochondrial permeability transition, Epac, mitochondria, adenylyl cyclase

## **Introduction**

Mitochondria are involved in cell life and fate decision through their multiple biological functions in energetic metabolism, reactive oxygen species (ROS) detoxification, cell growth and cell death <sup>1, 2, 3</sup>. In normal conditions, these functions are crucially regulated to provide sufficient energy for cell functions, maintain mitochondrial membrane integrity and avoid excessive cell death. This can be achieved by a plethora of cellular mechanisms controlling the mitochondrial mass and its turnover by mitophagy, oxidative phosphorylation, ROS production and detoxification, expression of pro- and anti-apoptotic proteins, prevention of mitochondrial membrane permeabilization (MMP) and/or post-translational modification of mitochondrial proteins such as phosphorylation, acetylation, carbonylation and ubiquitination <sup>4, 5</sup>. Moreover, mitochondria may participate in  $\text{Ca}^{2+}$  homeostasis via matrix  $\text{Ca}^{2+}$  accumulation through the mitochondrial  $\text{Ca}^{2+}$  uniporter (MCU),  $\text{Ca}^{2+}$  release into the cytosol and propagation to other mitochondria, notably in excitable cells <sup>6, 7, 8</sup>. In cardiomyocytes,  $\text{Ca}^{2+}$  movements between cytosol, sarcoplasmic reticulum and mitochondria are crucial for proper myofibril contraction and relaxation and energetic metabolism. Moreover, recent studies in cardiomyocyte-specific mutant mouse lacking the MCU showed a link between mitochondrial  $\text{Ca}^{2+}$  uptake and energetic supply in relation with cardiac workload during acute stress <sup>9, 10</sup>. In contrast, in many pathological conditions, excessive mitochondrial  $\text{Ca}^{2+}$  accumulation (i.e.  $\text{Ca}^{2+}$  overload), ROS production and adenine nucleotide depletion result in the sudden opening of a megachannel within the inner membrane (IM), namely the permeability transition pore complex. The prolonged opening of this unspecific pore (exclusion limit, 1.5 kDa), leads to the so-called mitochondrial permeability transition (MPT), cell death, inflammation and irreversible tissue damage <sup>11, 12</sup>. In humans and animal models, MPT can be a critical event in severe cardiac diseases such as ischemia-reperfusion injury, heart failure (HF) and radiation-induced cardiotoxicity <sup>11, 13, 14</sup>. Hence, MPT inhibition by

cyclosporin A has been shown to limit cardiac damages and improve cell survival. Inhibition of MPT has thus become an attractive therapeutic strategy in cardioprotection<sup>15</sup>.

Cyclic 3',5'-adenosine monophosphate (cAMP) is a major second messenger in many organs, particularly in the heart, where it regulates diverse physiological processes such as Ca<sup>2+</sup> homeostasis, beating frequency and myocardial contractility, as well as cell death<sup>16</sup>. Upon activation of heterotrimeric G<sub>s</sub> protein coupled receptors, such as β adrenergic receptors, transmembrane adenylyl cyclases (tmAC) produce cAMP in the bulk cytosol and in discrete compartments near the plasma membrane<sup>16</sup>. In the working myocardium, cAMP can activate two classes of effectors, namely protein kinase A (PKA) and/or the exchange protein directly activated by cAMP (Epac), which serves as exchange factor for small G proteins from the Ras family, Rap1 and Rap2, to mediate diverse biological effects<sup>17, 18, 19, 20</sup>. In the past few years, the development of several pharmacological agents targeting specifically Epac has contributed to demonstrate a key role for Epac in cardiac remodeling and hypertrophy<sup>21, 22</sup>. In addition to tmACs, cAMP can also be generated by soluble adenylyl cyclase (sAC), which is not regulated by heterotrimeric G proteins or forskolin, but can be activated by bicarbonate (HCO<sub>3</sub><sup>-</sup>) and Ca<sup>2+</sup><sup>16, 23, 24</sup>. sAC was found inside mitochondria in the brain and liver and in various mammalian cell types such as coronary endothelial cells, glomerula cells, tumor epithelial cells as well as neonatal cardiomyocytes<sup>25, 26, 27, 28, 29</sup>. In liver and brain, in response to HCO<sub>3</sub><sup>-</sup> and/or Ca<sup>2+</sup>, mitochondrial cAMP stimulates oxidative phosphorylation and ATP production<sup>30</sup>. In coronary endothelial cells, HCO<sub>3</sub><sup>-</sup> is transported into mitochondria and this leads to cAMP production by sAC, which indirectly modulates the cell fate through apoptosis<sup>31, 32</sup>. As a result, this pathway serves as a mechanism for metabolic adaptation to mitochondrial dysfunction induced by cytochrome c oxidase deficiency and could be a potential novel target to treat genetic mitochondrial diseases<sup>33</sup>. Altogether, these findings suggest that mitochondrial sAC functions as a metabolic sensor to stimulate mitochondrial

biological functions. If proven in primary cardiomyocytes, this intra-mitochondrial cAMP pathway might have clinical implication in HF as patients diagnosed with HF have markedly impaired mitochondrial metabolism and cAMP signaling, both contributing to cardiomyocyte dysfunction<sup>16, 34</sup>.

Intrigued by these previous findings, we tested the existence of a cAMP mitochondrial pathway in differentiated adult and neonatal cardiomyocytes and observed that genetic and/or pharmacological activation of this pathway prevents various cell death modalities such as apoptosis and necrosis. Our results also show that cardiac mitochondria isolated from adult rat hearts contain a truncated form of sAC (sAC<sub>t</sub>) as a source of cAMP as well as Epac1. A role of this local pathway is to control mitochondrial Ca<sup>2+</sup> entry through the MCU and to prevent the deleterious consequences of mitochondrial Ca<sup>2+</sup> overload such as dissipation of mitochondrial membrane potential ( $\Delta\Psi_m$ ) and induction of MPT. Interestingly, this mitochondrial sAC<sub>t</sub>-Epac1-MCU pathway remains functional in a rat model of HF induced by aortic stenosis and its activation prevents MPT.

## **Results**

### **Mitochondrial cAMP prevents cardiac cell death, apoptosis as well as necrosis**

To evaluate the capacity of sAC and cAMP to regulate the cardiomyocyte cell fate, we infected primary neonatal cardiomyocytes with two adenoviruses to overexpress the full length and the truncated sAC, sAC<sub>fl</sub> and sAC<sub>t</sub>, respectively, 24h before cell death induction by three different cell death inducers, i.e. camptothecin (CPT, 10  $\mu$ M, 48h), H<sub>2</sub>O<sub>2</sub> (300  $\mu$ M, 24h) and TNF  $\alpha$  + actinomycin D (10 ng/mL; 0.1  $\mu$ g/mL). We showed that the stimulation of endogenous sAC with HCO<sub>3</sub><sup>-</sup> as well as overexpression of sAC<sub>t</sub> prevented the various cell death modalities, apoptosis as well as necrosis measured by annexin/7-AAD fluorescent cell labeling (Figure 1a-b). Moreover, sAC<sub>fl</sub> protected from apoptosis induced by CPT and TNF $\alpha$

+ actinomycin D and necrosis induced by H<sub>2</sub>O<sub>2</sub>. In contrast, inhibition of sAC with 2-hydroxyestradiol (2HE), a sAC inhibitor<sup>29</sup> aggravated significantly cell death induced by camptothecin, H<sub>2</sub>O<sub>2</sub> as well as TNF  $\alpha$  + actinomycin D without any cytotoxicity alone (Figure 1 a). We observed also that cAMP protects from nuclei alterations measured by counting Hoechst-stained nuclei exhibiting morphologic and biochemical alterations, i.e. pycnosis and karyorrhexis (Figure 1c-f).

### **Mitochondrial sAC produces locally cAMP and regulates mitochondrial membrane potential ( $\Delta\Psi_m$ ) upon calcium overload**

Since mitochondria may be impermeant to cytosolic cAMP<sup>35</sup>, we decided to ascertain the expression of a functional endogenous sAC within cardiac mitochondria and evaluate mitochondrial cAMP levels in real time. To this end, we constructed an adenovirus encoding a cAMP sensitive FRET sensor (Epac-S<sup>H187</sup><sup>36</sup>) fused with a 4mt sequence and infected rat neonatal cardiomyocytes with this new targeted sensor, 4mt-Epac-S<sup>H187</sup>. The localization of 4mt-Epac-S<sup>H187</sup> in mitochondria was shown by co-localization of its green fluorescence with mitotracker red fluorescence (Pearson coefficient:  $0.92 \pm 0.02$ , n=6) (Figure 2a). Following infection with 4mt-Epac-S<sup>H187</sup>, we sequentially treated the cells with 24 mM HCO<sub>3</sub><sup>-</sup> to activate sAC, 25  $\mu$ M forskolin (FSK) to activate tmAC, and 20  $\mu$ M 8-CPT-2'-OMe-cAMP-AM (8CPT-cAMP AM), a permeant cAMP analogue to directly activate the sensor (Figure 2b). Addition of HCO<sub>3</sub><sup>-</sup> induced an increase in cAMP measured by 4mt-Epac-S<sup>H187</sup> (Figure 2b) which was virtually absent when the cells were infected with the cytoplasmic cAMP sensor Epac-S<sup>H187</sup> (Figure 2c). On the contrary, FSK induced a large response of cAMP measured with the cytoplasmic sensor (Figure 2c) and a smaller response of cAMP measured with the mitochondrial sensor (Figure 2b). These results are compatible with HCO<sub>3</sub><sup>-</sup> activating sAC in mitochondria and FSK increasing cAMP in the cytoplasm by activating tmAC. The

small response to FSK observed with 4mt-Epac-S<sup>H187</sup> might be due to incomplete targeting of the probe to mitochondria. Of note, 4mt-Epac-S<sup>H187</sup> has a much higher dynamic range than previously published sensors such as mito-EpacH90<sup>35</sup>, so that even a small expression of the probe in the cytosol would lead to a detectable signal. Alternatively, the small response to FSK measured with 4mt-Epac-S<sup>H187</sup> might be due to Ca<sup>2+</sup> stimulation of sAC in the matrix upon FSK stimulation as previously suggested<sup>29</sup>, or to a small permeability of the mitochondrial IM to cAMP. Interestingly, 2HE totally prevented the mitochondrial cAMP increase elicited by HCO<sub>3</sub><sup>-</sup> (Figure 2d). This confirms the involvement of a mitochondrial sAC as a source of cAMP in cardiomyocytes and eliminates possible artifact due to pH changes (all test solutions were continuously gassed with 95% O<sub>2</sub>/5% CO<sub>2</sub> maintaining pH at 7.4).

To address the role of sAC in the regulation of mitochondrial function, cardiomyocytes were transfected with siRNA control and siRNA against sAC for 48h. Next, they were loaded with the fluorescent  $\Delta\Psi_m$  indicator, TMRM, permeabilised and treated with Ca<sup>2+</sup>. The decrease in the level of sAC did not induce any changes of the mitochondrial network (Figure 2e-f). However, the measure of the ratio of TMRM fluorescence at 900 s (F) /the initial fluorescence (F0) showed that the silencing of sAC dramatically aggravated the loss of  $\Delta\Psi_m$  induced by Ca<sup>2+</sup>, suggesting a role of cAMP in  $\Delta\Psi_m$  control in stress conditions.

### **cAMP is produced by sACt in isolated mitochondria**

To further explore the local mitochondrial cAMP production without any contribution of components from other cellular compartments, we isolated subsarcolemmal mitochondria from rat heart ventricles by differential centrifugation and extensive washes<sup>37</sup>. First, we analyzed their morphology by transmission electron microscopy (Figure 3a) and their purity by western blotting (Figure 3b). As expected, mitochondria appeared round-shaped (mean

diameter, 0.8  $\mu\text{m}$ ) and presented numerous cristae, compatible with a high respiratory capacity. In comparison with rat ventricles homogenate (H), isolated mitochondria (M) were enriched in the adenine nucleotide translocase (ANT), an IM protein and almost not contaminated by cytosolic proteins such as GAPDH, myofibrillar proteins such as troponin I (TnI) and sarcoplasmic reticulum-associated proteins such as phospholamban (PLB) (Figure 3b). Using specific monoclonal antibodies, we detected the truncated form of sAC, namely sAC<sub>t</sub> (48 kDa) and the full-length form, sAC<sub>fl</sub> (187 kDa) in H fraction, whereas only the short form, which is the active form<sup>38</sup>, was found in the mitochondria preparation (Figure 3b). Next, we measured cAMP production in freshly isolated mitochondria by ELISA. We observed that HCO<sub>3</sub><sup>-</sup> and also, to a lesser extent, Ca<sup>2+</sup> stimulated cAMP production in a dose dependent manner and potentiated the response to ADP (Figure 3c). At 15 mM concentration, HCO<sub>3</sub><sup>-</sup> stimulated cAMP production by  $1.38 \pm 0.08$  fold ( $p < 0.05$ ) in the absence of ADP and by  $1.42 \pm 0.11$  fold ( $p < 0.01$ ) in the presence of ADP. While a small stimulatory effect of Ca<sup>2+</sup> on cAMP production was observed at 0.1  $\mu\text{M}$ , when increasing the concentration to 10  $\mu\text{M}$ , mitochondria lost their membrane potential (not shown), lowering drastically cAMP production (Figure 3c). Ca<sup>2+</sup> effects were abolished in the presence of RU360, confirming that the effect on cAMP levels is due to a specific uptake of Ca<sup>2+</sup> within the matrix. Similarly, when mitochondria were depolarized by the protonophore CCCP, no cAMP production was detected even in the presence of HCO<sub>3</sub><sup>-</sup> (Figure 3d). Moreover, 2HE reduced basal and fully blocked HCO<sub>3</sub><sup>-</sup>-stimulated cAMP production (Figure 3d). As a control, FSK had no stimulatory effect on cAMP in isolated mitochondria, confirming clearly the absence of tmAC within mitochondria (Figure 3d).

### **cAMP increases $\Delta\Psi\text{m}$ , respiration and ATP levels**

To understand the biological effects of the mitochondrial cAMP, we monitored the  $\Delta\Psi_m$  with the fluorescent probe, Rhod123, in the presence of various respiratory substrates for complex I (glutamate/malate), complex II and III (succinate), complex IV (TMPD + ascorbate) and their respective inhibitors, i.e. rotenone, antimycin A and sodium azide (Figure 3e-f). We used 1 mM 8Br-cAMP, a membrane permeant cAMP analogue, as a control, and 15 mM  $\text{HCO}_3^-$  to stimulate endogenous production of cAMP. Figure 3e shows that 8Br-cAMP slightly hyperpolarized mitochondria in condition of complex I-driven respiration (i.e. in the presence of glutamate/malate substrates), but failed to have any effect in the presence of respiratory substrates for complex II, III and IV. In contrast,  $\text{HCO}_3^-$  triggered a hyperpolarization in all conditions of substrates, the highest increase of  $\Delta\Psi_m$  being observed in condition of stimulation of complex I (Figure 3f). This hyperpolarization was accompanied by an increase in oxygen consumption in response to  $\text{HCO}_3^-$  (Figure 4a). Finally, when mitochondria were stimulated by  $\text{HCO}_3^-$  or  $\text{Ca}^{2+}$ , this led to an increase in ATP production both in the absence and presence of ADP (Figure 4b). These data indicate that cAMP produced by a mitochondrial sAC stimulates the oxidative phosphorylation increasing  $\Delta\Psi_m$  and mitochondrial ATP synthesis.

### **cAMP delays $\text{Ca}^{2+}$ -induced mitochondrial permeability transition (MPT)**

Based on the finding that cAMP is produced in cardiac mitochondria, we hypothesized that the cyclic nucleotide could have a role in the regulation of MPT, an essential pathophysiological process for the heart<sup>39</sup>. In cardiac isolated mitochondria, MPT can be elicited by 10  $\mu\text{M}$   $\text{Ca}^{2+}$  and prevented by 5  $\mu\text{M}$  cyclosporin A (CsA) and detected as a loss of  $\Delta\Psi_m$  and a matrix swelling<sup>37</sup>. We used two robust miniaturized assays<sup>37, 40</sup> to concomitantly measure the effect of sAC inhibition by 25  $\mu\text{M}$  2HE on mitochondrial depolarization (Figure 4c-d) and matrix swelling (Figure 4e-f) induced by 10  $\mu\text{M}$   $\text{Ca}^{2+}$ . sAC inhibition by 2HE

accelerated the depolarization (Figure 4c-d) and swelling (Figure 4e-f) induced by  $\text{Ca}^{2+}$ , as shown by the decreased half time of  $\Delta\Psi_m$  loss and swelling (Figure 4d-f). Conversely, 15 mM  $\text{HCO}_3^-$  slowed both processes (Figure 4d-f), suggesting that cAMP elevation confers a protection of mitochondria from  $\text{Ca}^{2+}$ -induced MPT.

### **Mitochondrial cAMP effects are independent of PKA**

cAMP effects are classically mediated by activation of two main effectors, PKA and Epac to regulate a plethora of biological functions in the heart<sup>19</sup>. In mitochondria, PKA has been reported to be associated with OM or to be in the matrix for controlling mitochondrial dynamics and oxidative metabolism<sup>35 41 42</sup>. We thus examined whether PKA was involved in the mitochondrial cAMP effects by testing the effects of two different pharmacological PKA inhibitors, H89 and KT5720, on the induction of MPT by  $\text{Ca}^{2+}$ . As shown in Supplementary Figure 1, these inhibitors, at concentrations ranging from 1 to 25  $\mu\text{M}$  for H89 and from 0.1 to 10  $\mu\text{M}$  for KT5720, had no significant effect on  $\Delta\Psi_m$  and swelling indicating that PKA may not be involved in MPT regulation.

### **Epac1 mediates cAMP effect on respiration and mitochondrial permeability transition.**

This prompted us to explore and dissect the possible role of Epac isoforms as effectors of the mitochondrial cAMP signaling pathway in isolated mitochondria. Then, we checked the expression of Epac isoforms. As shown in Figure 5a, both Epac1 and Epac2 isoforms were found in isolated cardiac mitochondria as well as in mitoplasts generated by osmotic shock, but were absent in the post-mitoplast supernatant. This suggests that Epac can be anchored to the IM facing the mitochondrial matrix or the intermembrane space or localized in the matrix. To evaluate the functional role of Epac, we used three pharmacological Epac inhibitors exhibiting different specificities and tested their effects on  $\text{Ca}^{2+}$ -induced depolarization and

swelling as well as oxygen consumption. We used ESI09, a pan Epac inhibitor, ESI05, an Epac2 selective inhibitor<sup>21,43</sup> and CE3F4, an Epac1 selective inhibitor<sup>44</sup>. As shown in Figure 5b, Epac1 inhibition with 50  $\mu$ M CE3F4 decreased basal oxygen consumption and also, prevented the stimulatory effect of  $\text{HCO}_3^-$ . Moreover, CE3F4 accelerated  $\text{Ca}^{2+}$ -induced depolarization (Figure 5c-d) and swelling (Figure 5e-f). Similar findings were obtained with ESI09 but not with ESI05 (Supplementary Figure 2). These data thus point to Epac1 as a key effector in mitochondrial cAMP effects.

Next, we tested the effect of Epac1 inhibition on the level of matrix  $\text{Ca}^{2+}$  in isolated mitochondria using the Rhod-2 fluorescent probe. To examine whether this effect was due to activation of  $\text{Ca}^{2+}$  extrusion or inhibition of  $\text{Ca}^{2+}$  entry, we examined whether Epac1 regulates the mitochondrial  $\text{Na}^+/\text{Ca}^{2+}$  exchanger (mNCX) or the mitochondrial  $\text{Ca}^{2+}$  uniporter (MCU) in the IM. As anticipated, 10  $\mu$ M CGP37157, a mNCX inhibitor, accelerated  $\text{Ca}^{2+}$  entry in isolated mitochondria (Figure 6c-d). This effect was similar to that of CE3F4. However, the combination of both inhibitors, each used at a concentration giving their maximal effect, produced an additive effect suggesting that they act *via* two distinct mechanisms. Similar results were obtained in the presence of  $\text{HCO}_3^-$  (Figure 6c-d). Thus, it is unlikely that Epac1 regulates mNCX. To examine the role of MCU, we used RU360, a highly specific MCU inhibitor. As anticipated, RU360 (from 0.2 to 1 nM) induced a dose-dependent inhibition of  $\text{Ca}^{2+}$  entry and  $\text{Ca}^{2+}$  accumulation (Supplementary Figure 3). Interestingly, inhibition of Epac in the presence of non-maximal concentrations of RU360 partially restored  $\text{Ca}^{2+}$  entry within mitochondria (Figure 6e-f, Supplementary Figure 3) but this effect was abrogated when the MCU was fully inhibited with 1 nM RU360 (Supplementary Figure 3a). These results suggest that MCU is the major effector of Epac1 for the regulation of mitochondrial  $\text{Ca}^{2+}$  movements.

**Epac1 mediates mitochondrial  $\text{Ca}^{2+}$  accumulation and  $\Delta\Psi_m$  loss in cardiomyocytes.** To recapitulate the above findings *in cellulo*, we tested the effect of Epac1 silencing by siRNA on the level of mitochondrial  $\Delta\Psi_m$  and matrix  $\text{Ca}^{2+}$  in neonatal cardiomyocytes with the fluorescent probes TMRM and Rhod2-AM. The results indicated that a decreased level of Epac1 in neonatal rats decreased  $\Delta\Psi_m$  (Figure 7a-c) and in parallel, accelerated the mitochondrial calcium entry (Figure 7d-e), as does the inhibitor CE3F4 in adult permeabilized cardiomyocytes upon addition of 200 nM  $\text{Ca}^{2+}$  (Figure 7 f-g). When used this concentration,  $\text{Ca}^{2+}$  did not affect mitochondrial  $\Delta\Psi_m$ , avoiding any artefact since most ions and metabolites transports are dependent of the  $\Delta\Psi_m$  (Supplementary Figure 4a-b). We also checked that our conditions of fluorescence excitation did not trigger MPT by testing the absence of modification of CE3F4 effects by CsA (Supplementary Figure 4c-d). Altogether, these results suggest that Epac1 plays a role in reducing the entry of  $\text{Ca}^{2+}$  in mitochondria and then, indirectly stabilizes the  $\Delta\Psi_m$  in primary cardiomyocytes.

### **The mitochondrial cAMP pathway can prevent MPT in HF rat model**

To evaluate the ability of the mitochondrial cAMP pathway to regulate MPT in a pathological model, we induced HF in rats by transverse aortic constriction (TAC) during 22 weeks<sup>45</sup>. As shown in Supplementary Figure 5a, TAC rats showed a strong cardiac and lung hypertrophy, which are characteristic features of HF. Accordingly, cardiac function was diminished as shown by echocardiography and the decrease in fractional shortening of the left ventricle (Supplementary Figure 5b-c). Expression level of various proteins was analyzed in heart ventricle homogenates and mitochondrial fraction by western-blot. As shown in Figure 8a-b,  $\text{sAC}_i$  protein expression was reduced and Epac1 expression was increased in homogenate and mitochondria from HF as compared to Sham hearts. MCU expression was similar in mitochondrial fraction from HF and Sham rats. To explore how HF affects mitochondrial

Ca<sup>2+</sup>-induced MPT, Ca<sup>2+</sup>-induced mitochondrial depolarization and Ca<sup>2+</sup> accumulation was measured in freshly isolated mitochondria from HF and Sham rats. As shown Figure 8c-d and Supplementary Figure 6a-d, 10 μM Ca<sup>2+</sup> induced a faster depolarization and Ca<sup>2+</sup> uptake in HF than in Sham mitochondria. In line with this, 10 μM Ca<sup>2+</sup> induced a faster mitochondrial swelling in HF than in Sham mitochondria (Figure 8e and Supplementary Figure 6e-f). This confirms that MPT is altered in HF, which could make mitochondria more vulnerable to Ca<sup>2+</sup> overload<sup>46</sup>. Interestingly, mitochondria from HF rats still responded to HCO<sub>3</sub><sup>-</sup> stimulation of mitochondrial cAMP production by sAC, by delaying ΔΨ<sub>m</sub> loss, Ca<sup>2+</sup> entry and MPT (i.e. matrix swelling). These effects were blunted by sAC or Epac1 inhibition with CE3F4 (Figure 8c-e and Supplementary Figure 6a-f).

## Discussion

In this study, we characterized a functional cAMP pathway within the mitochondria of neonatal and adult cardiomyocytes, which can regulate mitochondrial function and cell death. cAMP is locally produced within the mitochondria by a Ca<sup>2+</sup>/HCO<sub>3</sub><sup>-</sup> sensitive sAC<sub>t</sub> and activates Epac1 to stimulate oxidative metabolism while preventing MPT by limiting mitochondrial Ca<sup>2+</sup> accumulation via MCU. Since bicarbonate production can be catalyzed by carbonic anhydrase from CO<sub>2</sub> and H<sub>2</sub>O, CO<sub>2</sub> being produced by the Krebs cycle and the pyruvate dehydrogenase inside mitochondrial matrix, our data thus link, for the first time, mitochondrial metabolism, cAMP and cell death in the heart, independently of cytosolic cAMP signaling.

Our data are in good agreement with pioneer studies revealing the existence of a mitochondrial cAMP signaling in various cell types<sup>27,28,29</sup>. Prompted by the observation that a G protein- and forskolin (FSK)-insensitive sAC is present in various organelles<sup>38,47,48,49</sup>,

Acin-Perez *et al.* discovered a  $\text{CO}_2\text{-HCO}_3^-$ -sAC-cAMP-PKA (mito-sAC) signaling cascade entirely contained within mitochondria. This mito-sAC cascade serves as a metabolic sensor modulating ATP generation and ROS production in response to nutrient availability <sup>29</sup>. By targeting the recently developed Epac-S<sup>H187</sup> cAMP FRET sensor <sup>36</sup> to the mitochondria, we showed that sAC activation by  $\text{HCO}_3^-$  increases mitochondrial cAMP in neonatal cardiomyocytes, as shown earlier in HeLa and CHO cells <sup>35</sup>. Using organelle isolation followed by functional measurements (e.g. oxygen consumption, cAMP and ATP level measurements,  $\Delta\Psi\text{m}$ /swelling and calcium accumulation assays) and western-blots, we found that the constitutive mitochondrial cAMP signaling pathway regulates  $\Delta\Psi\text{m}$  and MPT not only in healthy but also in failing heart mitochondria and that these functions are mediated by Epac1.

*A functional mito-sAC pathway in mitochondria from adult heart.* Although it was already known that sAC can be localized into mitochondria <sup>47, 48, 49</sup>, little was known on their biological function in the organelle. Here, we identified endogenous sAC<sub>t</sub> in cardiac mitochondria and mitoplasts isolated from adult cardiomyocytes. We showed for the first time that increasing intra-mitochondrial cAMP level delays the onset of MPT, by increasing the half-time of  $\text{Ca}^{2+}$ -induced depolarization and matrix swelling, while stimulating oxygen consumption. Although  $\text{HCO}_3^-$  and  $\text{Ca}^{2+}$  enhanced cAMP production,  $\text{HCO}_3^-$  was more potent than  $\text{Ca}^{2+}$ , which is in line with the fact that  $\text{HCO}_3^-$  and  $\text{Ca}^{2+}$  stimulatory effects are not redundant:  $\text{HCO}_3^-$  modulates the active site of sAC, whereas  $\text{Ca}^{2+}$  increases ATP affinity <sup>27</sup>. Interestingly, a specific inhibitor of sAC, 2HE, totally prevented the effects of  $\text{HCO}_3^-$  and  $\text{Ca}^{2+}$  indicating that sAC may be the unique source of mitochondrial cAMP.

*Effectors of mitochondrial cAMP.* While PKA is the canonical mediator of cAMP in a number of cell functions and cell sub-compartments, and was shown earlier to regulate mitochondrial ATP and ROS production <sup>27, 29, 50, 51</sup>, PKA was clearly not involved in the induction of MPT

by  $\text{Ca}^{2+}$  since H89 and KT5720 failed to modulate it. We thus focused our interest on Epac, because it emerged in the last decade as another important player in cAMP signaling <sup>20</sup>. Although Epac possesses a mitochondrial-targeting sequence at its N terminus and has been shown to be localized inside mitochondria by heterologous expression <sup>52</sup>, to our knowledge there has been no report on a role for this protein in mitochondrial function. While the Epac2-selective inhibitor ESI05 had no effect, the non-selective inhibitor ESI09 or the Epac1-selective inhibitor CE3F4 antagonized the induction of MPT by  $\text{Ca}^{2+}$ . This indicates that Epac1 but not Epac2 is involved in the regulation of MPT. We found also that CE3F4 inhibits oxygen consumption stimulated or not by bicarbonate. Since the efficiency of CE3F4 to regulate oxygen consumption with a better efficiency than MPT, we speculate that Epac1 could have several targets, which remain to be identified, regulating differentially various mitochondrial functions.

In neonatal rat cardiomyocytes, silencing of Epac1 modulated the  $\text{Ca}^{2+}$  calcium entry and the  $\Delta\Psi_m$ . In the heart, Epac1 was recently shown to be localized and functionally involved also in nuclear signaling, whereas Epac2 is located at the T tubules and regulates arrhythmogenic sarcoplasmic reticulum  $\text{Ca}^{2+}$  leak <sup>53</sup>. Epac1 is the shortest isoform of Epac, being composed of five domains, with the C terminus domain CDC25-HD involved in the binding with Rap1 and Rap2 proteins, two members of the Ras small G protein family. While the intermediate downstream effector(s) of mitochondrial Epac1 still need to be identified, our results indicate that Epac1 activation may inhibit MCU activity. This hypothesis is supported by the fact that inhibition of MCU, but not of mNCX, mimics the effects of mitochondrial cAMP elevation in preventing MPT. Thus, we propose that activation of mitochondrial Epac1 protects the organelle from  $\text{Ca}^{2+}$  overload and from subsequent MPT via MCU modulation.

*Possible implications of the mitochondrial cAMP pathway for cell death and cardioprotection.*

$\text{Ca}^{2+}$  overload is considered as a conserved inducer of regulated cell death modalities

including apoptosis and necrosis, processes that lead ultimately to nuclear dismantling<sup>54</sup>. Using modulation of sAC by genetic and pharmacological manipulations in primary cardiomyocytes, our study demonstrates for the first time that activation of the mitochondrial cAMP pathway exerts an inhibition on MPT *in vitro* and on various cell death modalities, i.e. extrinsic and intrinsic apoptosis as well as necrosis. Conversely, pharmacological inhibition of sAC by 2HE increased dramatically nuclear damage and cell death. Thus, the targeted activation of this mitochondrial cAMP pathway may preserve cardiomyocytes from mitochondrial Ca<sup>2+</sup> overload and cell death *in vivo*. In that respect, in a pathological rat model of HF induced by pressure overload, which goes along with strong cardiac hypertrophy, cardiac function alteration, tissue remodeling, bioenergetics alterations and cardiomyocyte cell death<sup>45,46</sup>, sACt is down regulated and Epac1 is upregulated in mitochondria. However, the increase in Epac1 did not compensate the decrease of sACt in terms of function, suggesting that the level of cAMP is limiting for Epac1 in the control of MPT in cardiac mitochondria. Moreover, we found that the MPT alterations can be alleviated by stimulation of the mitochondrial cAMP pathway by HCO<sub>3</sub><sup>-</sup>. Thus, this new mitochondrial cAMP/sAC<sub>t</sub>/Epac1/MCU pathway might have potential therapeutic implications to regulate cell death in cardiac pathologies, such as HF and/or myocardial infarction<sup>54,55</sup>.

## **Material and methods**

Unless specified, all reagents and chemicals are from SIGMA Aldrich and of analytical grade.

### **Animals**

All animal care and experimental procedures conformed to the European Community guiding principles in the care and use of animals (Directive 2010/63/EU of the European Parliament) and authorizations to perform animal experiments according to this decree were obtained from the French Ministry of Agriculture, Fisheries and Food (No. D-92-283, 13 December

2012). All studies involving rats are reported in accordance with the ARRIVE guidelines for reporting experiments involving animals <sup>56</sup>. A total of 60 healthy, 4 Sham and 4 HF rats were used in the experiments described here.

### **Surgical procedure and echocardiography**

Male Wistar rats at three weeks of age (60–70 g; Janvier, Le Genest St Isle, France) were anesthetized with pentobarbital (60 mg/kg). The thoracic cage was opened and a stainless steel hemoclip was placed on the ascending aorta, to promote HF after 22 weeks, as previously described <sup>57</sup>. Sham-operated animals were used as controls. Cardiac structure and function was evaluated by echocardiography. Cardiac and pulmonary hypertrophy was determined as a ratio of organ weight to tibia length and to body weight <sup>57</sup>. Transthoracic two-dimensional-guided M-mode echocardiography of rats was performed using an echocardiograph with a 15 MHz Linear transducer (Vivid 9, General Electric Healthcare, Vélizy Villacoublay, France) under 3% isoflurane gas anesthesia and fractional release was calculated as described <sup>57</sup>.

### **Isolation of cardiac mitochondria**

Mitochondria were isolated from the heart of adult male Wistar rats at 8-10 weeks of age (275-375g; Janvier, Le Genest St Isle, France) as described <sup>37</sup>. Briefly, the heart was rapidly removed and placed into a cold buffer containing 0.3 M sucrose, 0.2 mM EGTA, 5 mM TES (pH 7.2). The heart was grinded with Polytron fastly and homogenized by using the Potter. The homogenate was centrifuged at 500 g for 10 min, 4°C. Then the supernatant was carefully removed and centrifuged again at 3,000 g for 10 min, 4°C. The pellets were washed in the isolation buffer and mitochondria kept on ice until use within 3h.

### **Mitochondrial transmembrane potential and swelling in isolated mitochondria**

Isolated mitochondria (25 µg proteins) were incubated with  $\text{Ca}^{2+}$  and drugs in 96 well microtiter plates<sup>37</sup>. Mitochondrial transmembrane potential ( $\Delta\Psi_m$ ) was measured using the fluorescent probe, rhodamine 123 (Rhod123, Excitation = 485 nm and Emission = 535 nm, Enzo Life Sciences, Villeurbanne, France) in a buffer containing 200 mM sucrose, 10 mM MOPS, 10 µM EGTA, 1 mM  $\text{H}_3\text{PO}_4$ , 5 mM succinate and 2 µM rotenone (pH 7.4) using Tecan Infinite 200 spectrofluorimeter. In parallel, matrix swelling was measured via light absorbance at 540 nm<sup>37</sup>.

### **Oxygen consumption**

Isolated mitochondria (50 µg proteins) were incubated with drugs in a buffer containing 250 mM sucrose, 30 mM  $\text{K}_2\text{HPO}_4$ , 1 mM EGTA, 5 mM  $\text{MgCl}_2$ , 15 mM KCl, and 1 mg/ml bovine serum albumin (BSA) (pH 7.4) supplemented with respiratory substrates and MitoXpress, an oxygen-sensitive phosphorescent dye (LUXCEL, Cork, Ireland). Oxygen consumption was measured in real time for 60 min at 30°C in 96-well plates using Tecan Infinite 200 (Excitation = 380 nm; Emission = 650 nm) in the presence of 1.65 mM ADP and with 5 mM malate and 12.5 mM glutamate<sup>37</sup>.

### **Mitochondrial $\text{Ca}^{2+}$ uptake in isolated mitochondria**

Isolated mitochondria (25 µg proteins) were incubated with 5 µM Rhod-2 (Enzo Life Sciences, Villeurbanne, France) in the buffer containing 200 mM sucrose, 10 mM MOPS, 10 µM EGTA, 1 mM  $\text{H}_3\text{PO}_4$ , 5 mM succinate and 2 µM rotenone for 30 min in dark at room temperature. After, the mitochondria were washed 2 times. Then the mitochondria were treated with various drugs for 10 min before applying  $\text{Ca}^{2+}$ . Fluorescence was measured in

real time for 60 min at room temperature in 96-well plates using Tecan Infinite 200 (Excitation =552 nm; Emission =581 nm).

### **cAMP measurements by ELISA**

cAMP measurements were performed according to manufacturer's instructions using monoclonal anti-cAMP antibody-based direct cAMP ELISA kit (New East Biosciences, King of Prussia, PA) on freshly isolated mitochondria from rat hearts (500µg proteins/sample) treated or not by  $\text{HCO}_3^-$ ,  $\text{Ca}^{2+}$  and  $\text{Ca}^{2+}$  + Ru360 for 20 min at room temperature before centrifugation and lysis. The sensitivity of cAMP detection is 29.6 fmol/mL<sup>58</sup>.

### **ATP measurements**

ATP measurements in isolated mitochondria were performed according to manufacturer's instructions using ATP Bioluminescence Assay kit CLSII (Roche).

### **Western blotting**

Total mitochondrial proteins were resolved on 4–15% Tris-glycine SDS-PAGE gels and electroblotted onto polyvinylidene fluoride (PVDF) membranes (Bio-Rad, Marnes La Coquette). Following electrotransfer, membranes were blocked for 1 h at room temperature in 5% BSA-PBST (10 mM Tris HCl, pH 8.0/150 mM NaCl/0.1% Tween 20). Next, membranes were incubated overnight at 4°C with primary antibody. The day after, the membranes were washed six times with PBST and incubated with peroxidase-conjugated secondary antibody at room temperature for 1 h. Peroxidase activity was detected with enhanced chemiluminescence (ECL Advance Western blotting detection kit; Thermo Scientific, Villebon sur Yvette, France). For protein detection, the following antibodies were used: sAC (Abcam, CEP

Biotech), Epac1, 2 (Cell signaling), ANT (Abcam), GAPDH (Cell signaling), VDAC (Genosphere), TnI (Cell signaling), PLB (Cell signaling) and MCU (Biorbyt).

### **Construction of mitochondria-targeted FRET sensor for cAMP**

The mitochondrial targeting sequence 4mt, encoding four copies of the signal sequence from subunit VIII of human cytochrome C oxidase, was amplified using the Advantage Polymerase (Clontech) and primers F (ACTATAGGGAGACCCAAGCTTATG) and R (TGGTGGCGGCAAGCTTCTTGCTCACCATGGTGGC). The pcDNA-4mt-D3-cpv vector used as a matrix for amplification of 4mt was a kind gift from Dr. Roger Tsien (HHMI investigator at the University of California San Diego, USA). The PCR fragment was cloned into the HindIII restriction site of pcDNA3-Epac-S<sup>H187</sup> using the Infusion HD Cloning system (Clontech). Epac-S<sup>H187</sup> encodes for a fourth generation Epac1-based cAMP sensor and was a kind gift from Dr. Kees Jalink (The Netherlands Cancer Institute, Amsterdam, Netherlands)<sup>36</sup>. Once the pcDNA-4mt-Epac-S<sup>H187</sup> vector was amplified in Stellar *E. coli* (Clontech) bacteria, its identity with parental sequences was verified by PCR using primers F (ACTCACTATAGGGAGACC) and R (TGCGGCCGCCATGGTGGC), and DNA double strand sequencing (INSERM U1056 – UMR 5165 CNRS UPS – UDEAR, Toulouse, France). Adenoviruses encoding Epac-S<sup>H187</sup> and 4mt-Epac-S<sup>H187</sup> were generated by Welgen, Inc.

### **Cardiomyocyte isolation, adenoviral infection and cell death evaluation**

Adult and neonatal cardiomyocytes were isolated as previously described<sup>59 60</sup>. For FRET experiments, neonatal cardiomyocytes were plated on 35 mm, laminin-coated culture dishes (10 µg/mL) at a density of  $4 \times 10^5$  cells per dish. The day after, cells were infected with Epac-S<sup>H187</sup> and 4mt-Epac-S<sup>H187</sup> adenoviruses in Opti-MEM<sup>®</sup> (Life technologies, St Aubin, France) for 48h. Similarly, adenoviruses expressing sACt and sACfl were used (generous gift of Pr.

M. Conti, University of California, San Francisco, CA, USA). For confocal microscopy experiments, adult cardiomyocytes were plated on 35 mm, laminin-coated culture dishes (10 $\mu$ g/mL) at a density of 2 $\times$ 10<sup>4</sup> cells per dish. For cell death evaluation, neonatal cells were stained with Apoptosis/Necrosis Detection Kit (Abcam) for 1h at room temperature as described by the manufacturer.

### **siRNA transfection to knockdown sAC and Epac1**

On-Target plus SMART pool siRNA, a mixture of four siRNA provided as a single reagent were purchased from Dharmacon. At day 0, neonatal cardiomyocytes were plated overnight on 35 mm, laminin-coated culture dishes (10  $\mu$ g/mL) at 4  $\times$  10<sup>5</sup>. At day 1, the cells were transfected with 50 nM sAC/Epac1 or non-targeting control siRNA using Lipofectamine® RNAi MAX Transfection Reagent for 48 h.

### **Mitochondrial transmembrane potential measurement in neonatal cardiomyocytes**

Isolated rat cardiomyocytes were loaded with 100 nM TMRM at 37°C for 15 min. After, the sarcolemmal membrane was permeabilized by perfusion of digitonin (5  $\mu$ g/mL) in a Ca<sup>2+</sup> free internal solution that contained 50 mM KCl, 80 mM potassium aspartate, 4 mM sodium pyruvate, 20 mM HEPES, 3 mM MgCl<sub>2</sub>, 3 mM Na<sub>2</sub>ATP, 5.8 mM glucose, and 0.5 mM EGTA (pH 7.3 with KOH). Then the free Ca<sup>2+</sup> concentration in the internal solution was increased to 200 nM. The Ca<sup>2+</sup> was calculated using the maxchelator program from Stanford. Images were acquired with a Leica (SP5) confocal microscope. Excitation was achieved by a white light laser fitted at 549 nm and emission collected at 570 nm. Analyses were made with Image J program.

### **Measurement of mitochondrial Ca<sup>2+</sup> in cardiomyocytes**

Isolated neonatal or adult rat cardiomyocytes were loaded with 5  $\mu\text{M}$  Rhod-2 at 37°C for 30 min. To remove cytosolic Rhod-2, the sarcolemmal membrane was permeabilized by perfusion of digitonin (5  $\mu\text{g}/\text{mL}$ ) in a  $\text{Ca}^{2+}$  free internal solution that contained 50 mM KCl, 80 mM potassium aspartate, 4 mM sodium pyruvate, 20 mM HEPES, 3 mM  $\text{MgCl}_2$ , 3 mM  $\text{Na}_2\text{ATP}$ , 5.8 mM glucose, and 0.5 mM EGTA (pH 7.3 with KOH). After the sarcolemmal membrane was permeabilized, the free  $\text{Ca}^{2+}$  concentration in the internal solution was increased to 200 nM. The  $\text{Ca}^{2+}$  was calculated using the maxchelator program from Stanford. Images were acquired with a Leica (SP5) confocal microscope. Excitation was achieved by a white light laser fitted at 552 nm and emission collected at 575 nm. Analyses were made with Image J program.

#### **Fluorescence resonance energy transfer measurements of cAMP levels**

Fluorescence resonance energy transfer (FRET) imaging experiments were performed 48h after infection of neonatal cardiomyocytes. Cells were bathed in HEPES-buffered Ringer's solution containing: 125 mM NaCl, 25 mM HEPES, 10 mM glucose, 5 mM  $\text{K}_2\text{HPO}_4$ , 1 mM  $\text{MgSO}_4$ , and 1 mM  $\text{CaCl}_2$ , pH 7.4. For sAC activation by  $\text{HCO}_3^-$ , the medium was the Krebs-Henseleit solution containing : 120 mM NaCl, 2.09 mM  $\text{K}_2\text{HPO}_4$ , 0.34 mM  $\text{KH}_2\text{PO}_4$ , 24 mM  $\text{NaHCO}_3$ , 1 mM  $\text{MgSO}_4$ , 1 mM  $\text{CaCl}_2$ , and 10 mM D-glucose. Krebs-Henseleit solution was gassed continuously with 95%  $\text{O}_2$ /5%  $\text{CO}_2$  to maintain a pH of 7.4<sup>35</sup>. Real-time FRET experiments were performed at room temperature. Images were captured every 5 s using the 40 $\times$  oil immersion objective of an inverted microscope (Nikon) connected to a Cool SNAP HQ2 camera (Photometrics) controlled by the Metafluor software (Molecular Devices). The donor (mTurquoise2)<sup>36</sup> was excited during 300 ms by a Xenon lamp (Nikon) using a 440/20BP filter and a 455LP dichroic mirror. Dual-emission imaging of donor and acceptor

was performed using a Dual-View emission splitter equipped with a 510 LP dichroic mirror and BP filters 480/30 and 535/ 25 nm, respectively.

### **Data Analysis**

Results are expressed as mean  $\pm$  SEM. The Origin software was used for statistical analysis. Differences between groups have been analyzed by one-way ANOVA and Student *t* test. A value of  $p < 0.05$  were considered as statistically significant. The number of animals, cells and independent experiments performed is indicated in the figure legends.

### **Conflict of Interest**

The authors declare no conflict of interest.

### **Acknowledgments**

This work has been funded by INSERM (AMG, CB, GV, RF), the Investment for the Future program ANR-11-IDEX-0003-01 within the LABEX ANR-10-LABX-0033 (CB, GV, RF) and ANR (ANR-13-ISV1-0001-01, CB). Zhenyu WANG is supported by a fellowship from the China Scholarship Council. The Leica microscope was funded by CORDDIM (Investissement 2010, COD100296). Authors wish to thank Florence Lefebvre for her assistance in adult cardiomyocytes isolation and Valérie Domergue for animal housing and care at the Animex facility, IPSIT, Châtenay-Malabry, France. Authors also thank Christine Longin for Transmission Electron Microscopy at INRA, Jouy-en-Josas, France. We thank Jessica Sabourin, Cécile Martel, Delphine Mika and Jérôme Leroy for helpful discussions.

## References

1. Green DR, Reed JC. Mitochondria and apoptosis. *Science* 1998, **281**(5381): 1309-1312.
2. Brenner C, Kroemer G. Apoptosis. Mitochondria--the death signal integrators. *Science* 2000, **289**(5482): 1150-1151.
3. Desagher S, Martinou JC. Mitochondria as the central control point of apoptosis. *Trends in cell biology* 2000, **10**(9): 369-377.
4. Kroemer G, Galluzzi L, Brenner C. Mitochondrial membrane permeabilization in cell death. *Physiological reviews* 2007, **87**: 99-163.
5. Duchen MR, Szabadkai G. Roles of mitochondria in human disease. *Essays in biochemistry* 2010, **47**: 115-137.
6. Ichas F, Jouaville L, Mazat J. Mitochondria are excitable organelles capable of generating and conveying electrical and calcium signals. *Cell* 1997, **89**: 1145-1153.
7. Rizzuto R, Pozzan T. Microdomains of intracellular Ca<sup>2+</sup>: molecular determinants and functional consequences. *Physiol Rev* 2006, **86**: 369-408.
8. Viola HM, Hool LC. Cross-talk between L-type Ca<sup>2+</sup> channels and mitochondria. *Clinical and experimental pharmacology & physiology* 2010, **37**(2): 229-235.
9. Luongo TS, Lambert JP, Yuan A, Zhang X, Gross P, Song J, *et al.* The Mitochondrial Calcium Uniporter Matches Energetic Supply with Cardiac Workload during Stress and Modulates Permeability Transition. *Cell reports* 2015, **12**: 23-34.
10. Kwong JQ, Lu X, Correll RN, Schwanekamp JA, Vagnozzi RJ, Sargent MA, *et al.* The Mitochondrial Calcium Uniporter Selectively Matches Metabolic Output to Acute Contractile Stress in the Heart. *Cell reports* 2015, **12**: 15-22.
11. Griffiths EJ, Halestrap AP. Mitochondrial non-specific pores remain closed during cardiac ischaemia, but open upon reperfusion. *Biochem J* 1995, **307** (Pt 1): 93-98.
12. Halestrap AP, Richardson AP. The mitochondrial permeability transition: A current perspective on its identity and role in ischaemia/reperfusion injury. *J Mol Cell Cardiol* 2015, **78C**: 129-141.
13. Boerma M. Experimental radiation-induced heart disease: past, present, and future. *Radiation research* 2012, **178**(1): 1-6.
14. Kwong JQ, Molkenin JD. Physiological and pathological roles of the mitochondrial permeability transition pore in the heart. *Cell metabolism* 2015, **21**(2): 206-214.
15. Piot C, Croisille P, Staat P, Thibault H, Rioufol G, Mewton N, *et al.* Effect of cyclosporine on reperfusion injury in acute myocardial infarction. *The New England journal of medicine* 2008, **359**(5): 473-481.

16. Guellich A, Mehel H, Fischmeister R. Cyclic AMP synthesis and hydrolysis in the normal and failing heart. *Pflugers Archiv : European journal of physiology* 2014, **466**: 1163-1175.
17. de Rooij J, Zwartkruis FJ, Verheijen MH, Cool RH, Nijman SM, Wittinghofer A, *et al.* Epac is a Rap1 guanine-nucleotide-exchange factor directly activated by cyclic AMP. *Nature* 1998, **396**(6710): 474-477.
18. Kawasaki H, Springett GM, Toki S, Canales JJ, Harlan P, Blumenstiel JP, *et al.* A Rap guanine nucleotide exchange factor enriched highly in the basal ganglia. *Proceedings of the National Academy of Sciences of the United States of America* 1998, **95**(22): 13278-13283.
19. Schmidt M, Dekker FJ, Maarsingh H. Exchange protein directly activated by cAMP (epac): a multidomain cAMP mediator in the regulation of diverse biological functions. *Pharmacological reviews* 2013, **65**(2): 670-709.
20. Metrich M, Berthouze M, Morel E, Crozatier B, Gomez AM, Lezoualc'h F. Role of the cAMP-binding protein Epac in cardiovascular physiology and pathophysiology. *Pflugers Archiv : European journal of physiology* 2010, **459**(4): 535-546.
21. Chen H, Wild C, Zhou X, Ye N, Cheng X, Zhou J. Recent advances in the discovery of small molecules targeting exchange proteins directly activated by cAMP (EPAC). *Journal of medicinal chemistry* 2014, **57**(9): 3651-3665.
22. Parnell E, Palmer TM, Yarwood SJ. The future of EPAC-targeted therapies: agonism versus antagonism. *Trends in pharmacological sciences* 2015, **36**(4): 203-214.
23. Litvin TN, Kamenetsky M, Zarifyan A, Buck J, Levin LR. Kinetic properties of "soluble" adenylyl cyclase. Synergism between calcium and bicarbonate. *The Journal of biological chemistry* 2003, **278**(18): 15922-15926.
24. Jaiswal BS, Conti M. Calcium regulation of the soluble adenylyl cyclase expressed in mammalian spermatozoa. *Proceedings of the National Academy of Sciences of the United States of America* 2003, **100**(19): 10676-10681.
25. Spät A, Katona D, Rajki A, Di Benedetto G, Pozzan T. Calcium-dependent mitochondrial cAMP production enhances aldosterone secretion. *Mol Cell Endocrinol* 2015, **pii**: S0303-7207.
26. Kamenetsky M, Middelhaufe S, Bank EM, Levin LR, Buck J, Steegborn C. Molecular details of cAMP generation in mammalian cells: a tale of two systems. *J Mol Biol* 2006, **362**(4): 623-639.
27. Acin-Perez R, Salazar E, Kamenetsky M, Buck J, Levin LR, Manfredi G. Cyclic AMP produced inside mitochondria regulates oxidative phosphorylation. *Cell metabolism* 2009, **9**(3): 265-276.

28. Zippin JH, Levin LR, Buck J. CO<sub>2</sub>/HCO<sub>3</sub><sup>-</sup>-responsive soluble adenylyl cyclase as a putative metabolic sensor. *Trends in endocrinology and metabolism: TEM* 2001, **12**(8): 366-370.
29. Di Benedetto G, Scalzotto E, Mongillo M, Pozzan T. Mitochondrial Ca<sup>2+</sup> Uptake Induces Cyclic AMP Generation in the Matrix and Modulates Organelle ATP Levels. *Cell metabolism* 2013, **17**(6): 965-975.
30. Acin-Perez R, Russwurm M, Gunnewig K, Gertz M, Zoidl G, Ramos L, *et al.* A phosphodiesterase 2A isoform localized to mitochondria regulates respiration. *J Biol Chem* 2011, **286**(35): 30423-30432.
31. Kumar S, Flacke JP, Kostin S, Appukuttan A, Reusch HP, Ladilov Y. SLC4A7 sodium bicarbonate co-transporter controls mitochondrial apoptosis in ischaemic coronary endothelial cells. *Cardiovascular research* 2011, **89**(2): 392-400.
32. Kumar S, Kostin S, Flacke JP, Reusch HP, Ladilov Y. Soluble adenylyl cyclase controls mitochondria-dependent apoptosis in coronary endothelial cells. *The Journal of biological chemistry* 2009, **284**(22): 14760-14768.
33. Acin-Perez R, Salazar E, Brosel S, Yang H, Schon EA, Manfredi G. Modulation of mitochondrial protein phosphorylation by soluble adenylyl cyclase ameliorates cytochrome oxidase defects. *EMBO molecular medicine* 2009, **1**(8-9): 392-406.
34. Neubauer S. The failing heart--an engine out of fuel. *N Engl J Med* 2007 **356**: 1140-1151.
35. Lefkimmiatis K, Leronni D, Hofer AM. The inner and outer compartments of mitochondria are sites of distinct cAMP/PKA signaling dynamics. *The Journal of cell biology* 2013, **202**(3): 453-462.
36. Klarenbeek J, Goedhart J, van Batenburg A, Groenewald D, Jalink K. Fourth-generation epac-based FRET sensors for cAMP feature exceptional brightness, photostability and dynamic range: characterization of dedicated sensors for FLIM, for ratiometry and with high affinity. *PloS one* 2015, **10**(4): e0122513.
37. Wang Z, Nicolas C, Fischmeister R, Brenner C. Enzymatic assays for probing mitochondrial apoptosis. *Methods Mol Biol* 2015, **1265**: 407-414.
38. Buck J, Sinclair ML, Schapal L, Cann MJ, Levin LR. Cytosolic adenylyl cyclase defines a unique signaling molecule in mammals. *Proceedings of the National Academy of Sciences of the United States of America* 1999, **96**(1): 79-84.
39. Brenner C, Moulin M. Physiological roles of the permeability transition pore. *Circ Res* 2012 **111**: 1237-1247.
40. Belzacq-Casagrande AS, Martel C, Pertuiset C, Borgne-Sanchez A, Jacotot E, Brenner C. Pharmacological screening and enzymatic assays for apoptosis. *Frontiers in bioscience : a journal and virtual library* 2009, **14**: 3550-3562.

41. Sardanelli AM, Technikova-Dobrova Z, Scacco SC, Speranza F, Papa S. Characterization of proteins phosphorylated by the cAMP-dependent protein kinase of bovine heart mitochondria. *FEBS letters* 1995, **377**(3): 470-474.
42. Carlucci A, Lignitto L, Feliciello A. Control of mitochondria dynamics and oxidative metabolism by cAMP, AKAPs and the proteasome. *Trends in cell biology* 2008, **18**(12): 604-613.
43. Chen H, Ding C, Wild C, Liu H, Wang T, White MA, *et al.* Efficient Synthesis of ESI-09, A Novel Non-cyclic Nucleotide EPAC Antagonist. *Tetrahedron letters* 2013, **54**(12): 1546-1549.
44. Courilleau D, Bouyssou P, Fischmeister R, Lezoualc'h F, Blondeau JP. The (R)-enantiomer of CE3F4 is a preferential inhibitor of human exchange protein directly activated by cyclic AMP isoform 1 (Epac1). *Biochemical and biophysical research communications* 2013, **440**(3): 443-448.
45. Joubert F, Wilding JR, Fortin D, Domergue-Dupont V, Novotova M, Ventura-Clapier R, *et al.* Local energetic regulation of sarcoplasmic and myosin ATPase is differently impaired in rats with heart failure. *The Journal of physiology* 2008, **586**(Pt 21): 5181-5192.
46. Marcil M, Ascah A, Matas J, Bélanger S, Deschepper C, Burelle Y. Compensated volume overload increases the vulnerability of heart mitochondria without affecting their functions in the absence of stress. *J Mol Cell Cardiol* 2006, **41**: 998-1009.
47. Zippin JH, Chen Y, Nahirney P, Kamenetsky M, Wuttke MS, Fischman DA, *et al.* Compartmentalization of bicarbonate-sensitive adenylyl cyclase in distinct signaling microdomains. *FASEB journal : official publication of the Federation of American Societies for Experimental Biology* 2003, **17**(1): 82-84.
48. Sulimovici S, Lunenfeld B. Effect of gonadotrophins on adenylyl cyclase of the outer and inner membrane subfractions of rat testis mitochondria. *FEBS letters* 1974, **41**(2): 345-347.
49. Fine AS, Egnor RW, Forrester E, Stahl SS. Adenylyl cyclase localization in unfixed specimens of rat oral mucosa and isolated mitochondria. *The journal of histochemistry and cytochemistry : official journal of the Histochemistry Society* 1982, **30**(11): 1171-1178.
50. Papa S, De Rasmio D, Scacco S, Signorile A, Technikova-Dobrova Z, Palmisano G, *et al.* Mammalian complex I: a regulable and vulnerable pacemaker in mitochondrial respiratory function. *Biochimica et biophysica acta* 2008, **1777**(7-8): 719-728.
51. Acin-Perez R, Gatti DL, Bai Y, Manfredi G. Protein phosphorylation and prevention of cytochrome oxidase inhibition by ATP: coupled mechanisms of energy metabolism regulation. *Cell metabolism* 2011, **13**(6): 712-719.

52. Qiao J, Mei FC, Popov VL, Vergara LA, Cheng X. Cell cycle-dependent subcellular localization of exchange factor directly activated by cAMP. *The Journal of biological chemistry* 2002, **277**(29): 26581-26586.
53. Pereira L, Rehmann H, Lao DH, Erickson JR, Bossuyt J, Chen J, *et al.* Novel Epac fluorescent ligand reveals distinct Epac1 vs. Epac2 distribution and function in cardiomyocytes. *Proceedings of the National Academy of Sciences of the United States of America* 2015, **112**(13): 3991-3996.
54. Galluzzi L, Bravo-San Pedro JM, Vitale I, Aaronson SA, Abrams JM, Adam D, *et al.* Essential versus accessory aspects of cell death: recommendations of the NCCD 2015. *Cell death and differentiation* 2015, **22**(1): 58-73.
55. Kung G, Konstantinidis K, Kitsis RN. Programmed necrosis, not apoptosis, in the heart. *Circulation research* 2011, **108**(8): 1017-1036.
56. Kilkenny C, Browne W, Cuthill IC, Emerson M, Altman DG. Animal research: reporting in vivo experiments: the ARRIVE guidelines. *British journal of pharmacology* 2010, **160**(7): 1577-1579.
57. Hubert F, Belacel-Ouari M, Manoury B, Zhai K, Domergue-Dupont V, Mateo P, *et al.* Alteration of vascular reactivity in heart failure: role of phosphodiesterases 3 and 4. *British journal of pharmacology* 2014, **171**(23): 5361-5375.
58. Chen Y, Cann MJ, Litvin TN, Iourgenko V, Sinclair ML, Levin LR, *et al.* Soluble adenylyl cyclase as an evolutionarily conserved bicarbonate sensor. *Science* 2000, **289**(5479): 625-628.
59. Morel E, Marcantoni A, Gastineau M, Birkedal R, Rochais F, Garnier A, *et al.* cAMP-binding protein Epac induces cardiomyocyte hypertrophy. *Circulation research* 2005, **97**(12): 1296-1304.
60. Rochais F, Vandecasteele G, Lefebvre F, Lugnier C, Lum H, Mazet J, *et al.* Negative feedback exerted by cAMP-dependent protein kinase and cAMP phosphodiesterase on subsarcolemmal cAMP signals in intact cardiac myocytes: an in vivo study using adenovirus-mediated expression of CNG channels. *The Journal of biological chemistry* 2004, **279**: 52095-52105.

### Legend to figures

**Figure 1. Mitochondrial cAMP protects cell death induced by camptothecin (CPT), H<sub>2</sub>O<sub>2</sub> and TNF $\alpha$  in neonatal cardiomyocytes. (a)** Cells were treated with vehicle, 15 mM HCO<sub>3</sub><sup>-</sup>

and 25  $\mu\text{M}$  2HE in the presence of 10  $\mu\text{M}$  CPT for 48h or 300  $\mu\text{M}$   $\text{H}_2\text{O}_2$  for 24h or 10ng/mL  $\text{TNF}\alpha$ /0.1  $\mu\text{g}/\text{mL}$  actinomycin D for 24h. **(b)** Cells were infected by adenoviruses encoding  $\beta$ -gal,  $\text{sAC}_i$  and  $\text{sAC}_n$  for 24h and then treated with 10  $\mu\text{M}$  CPT for 48h or 300  $\mu\text{M}$   $\text{H}_2\text{O}_2$  for 24h or 10ng/mL  $\text{TNF}\alpha$ /0.1  $\mu\text{g}/\text{mL}$  actinomycin D for 24h. \* $P$ <0.05, \*\*  $P$ <0.01 versus vehicle or  $\beta$ -gal viability; # $P$ <0.05, ### $P$ <0.01 versus vehicle or  $\beta$ -gal apoptosis; \$ $P$ <0.05, \$\$ $P$ <0.01 versus vehicle or  $\beta$ -gal necrosis (n=3). **(c)** Representative fluorescence images of nuclear staining with Hoechst 33342. **(d, e, f)** Quantitative analysis of cell death rate. Cells were infected with adenoviruses encoding  $\beta$ -gal,  $\text{sAC}_i$  and  $\text{sAC}_n$  for 24h and then treated with CPT (10  $\mu\text{M}$ ) for 48h,  $\text{H}_2\text{O}_2$  (300  $\mu\text{M}$ ) or  $\text{TNF}\alpha$ /actinomycin D (10 ng/mL, 0.1  $\mu\text{g}/\text{mL}$ ) for 24h. Or Cells were treated with vehicle, 15 mM  $\text{HCO}_3^-$  and 25  $\mu\text{M}$  2HE in the presence of CPT (10  $\mu\text{M}$ ) for 48h,  $\text{H}_2\text{O}_2$  (300  $\mu\text{M}$ ) or  $\text{TNF}\alpha$ /actinomycin D (10 ng/mL, 0.1 $\mu\text{g}/\text{mL}$ ) for 24h. \* $P$ <0.05, \*\* $P$ <0.01, \*\*\* $P$ <0.001 versus  $\beta$ -gal; # $P$ <0.05, ### $P$ <0.01, #### $P$ <0.001 versus vehicle (n=3).

**Figure 2. Mitochondrial sACt produces locally cAMP and regulates mitochondrial membrane potential ( $\Delta\Psi_m$ ) upon calcium overload.** **(a)** Mitochondrial localization of the 4mt-Epac-S<sup>H187</sup> cAMP sensor in rat isolated neonatal cardiomyocytes. Confocal images of cardiomyocytes infected with 4mt-Epac-S<sup>H187</sup> (green) and stained with MitoTracker Red. The co-localization of 4mt-Epac-S<sup>H187</sup> with MitoTracker is shown in yellow. Bar scale, 10  $\mu\text{m}$ . **(b, c)** Representative kinetics of percentage increase in CFP/YFP recorded in rat neonatal cardiomyocytes infected with either 4mt-Epac-S<sup>H187</sup> **(b)** or Epac-S<sup>H187</sup> sensor **(c)** and sequentially stimulated with 24 mM  $\text{HCO}_3^-$ , 25  $\mu\text{M}$  forskolin (FSK) and 20  $\mu\text{M}$  8CPT-cAMP AM. **(d)** Representative kinetics of percentage increase in CFP/YFP recorded in rat neonatal cardiomyocytes infected with 4mt-Epac-S<sup>H187</sup> exposed to 25  $\mu\text{M}$  2HE in the absence or presence of 24 mM  $\text{HCO}_3^-$ , and finally to 20  $\mu\text{M}$  8CPT-cAMP AM (B, n=19; C, n=6; D, n=7). **(e)** sAC expression in neonatal rat cardiomyocytes transfected with non-targeting siRNA (si-Control) or sAC siRNA (si-sAC). **(f)** Representative confocal images of TMRM-labeled permeabilized neonatal rat cardiomyocytes transfected with si-Control or si-sAC at time 0 s (left) and 900 s (right) after  $\text{Ca}^{2+}$  (600 nM) addition. Bar scale, 50  $\mu\text{m}$ . **(g)** Averaged values of mitochondrial membrane potential (measured as F/F0 where F is the TMRM fluorescence signal at 900 s and F0 is the signal at time 0 s of  $\text{Ca}^{2+}$  addition) (n=50). \*\* $P$ <0.01 versus si-Control.

**Figure 3. cAMP produced by soluble adenylate cyclase (sAC) regulates mitochondrial transmembrane inner potential ( $\Delta\Psi_m$ ).** **(a)** Transmission electron microscopy image of isolated subsarcolemmal mitochondria from rat heart ventricles. Bar scale, 1  $\mu\text{m}$ . **(b)** Purity analysis of mitochondrial fraction by western-blot. Proteins ANT, inner membrane; GAPDH, cytosol; PLB, sarcoplasmic reticulum; TnI, myofibrils; full length sAC ( $\text{sAC}_n$ ) and truncated sAC ( $\text{sAC}_i$ ) were detected in heart homogenate (H) and mitochondria (M). Results are representative of 3 independent experiments. **(c)** cAMP levels produced in isolated mitochondria in the presence of  $\text{HCO}_3^-$ ,  $\text{Ca}^{2+}$  and  $\text{Ca}^{2+}$  + Ru360 (MCU inhibitor, 1nM), under basal condition or upon stimulation with 1.65 mM ADP, determined by ELISA (n=4-5). **(d)** cAMP levels in isolated mitochondria under basal condition or in the presence of 15 mM  $\text{HCO}_3^-$ , 25  $\mu\text{M}$  2HE,  $\text{HCO}_3^-$  + 2HE, 25  $\mu\text{M}$  FSK, 5 $\mu\text{M}$  CCCP or CCCP +  $\text{HCO}_3^-$ , determined by ELISA. Control, untreated mitochondria; ns, not significant (n=3-7). **(e)**  $\Delta\Psi_m$  was evaluated with Rhod 123 fluorescence in the absence or presence of 1 mM 8Br-cAMP or 15 mM  $\text{HCO}_3^-$  in isolated cardiac mitochondria with different respiratory substrates: 0.25 mM malate (M) and 0.5 mM glutamate (G) for complex I (inhibited by 2  $\mu\text{M}$  rotenone, Rot); 0.5 mM succinate (Succ) for complex II and III (blocked by the complex III inhibitor antimycin

A, AA, 0.25  $\mu\text{g/mL}$ ) and 0.05 mM TMPD (T) with 0.2 mM ascorbate (A) for complex IV (inhibited by 5 mM sodium azide). RFU, relative fluorescence unit. **(f)** Comparison of 8Br-cAMP and bicarbonate effects on  $\Delta\Psi\text{m}$  stimulated with various respiratory substrates. Areas under the curve (AUC) were calculated from experiments such as shown in **(e)** ( $n=3$ ). AU, arbitrary units. \* $P<0.05$ , \*\* $P<0.01$ , \*\*\* $P<0.001$  versus control; #  $P<0.05$ , ##  $P<0.01$  versus control with ADP.

**Figure 4. cAMP regulates mitochondrial respiration, ATP levels and  $\text{Ca}^{2+}$  induced mitochondrial depolarization and swelling.** **(a)** Oxygen consumption of mitochondria measured with the probe MitoXpress in the presence or absence of 15 mM  $\text{HCO}_3^-$  driven by 2.5 mM malate and 5 mM glutamate with 1.65 mM ADP. Control was normalized at 100% ( $n=5$ ). **(b)** ATP production in the presence of 15 mM  $\text{HCO}_3^-$  and 0.1  $\mu\text{M}$   $\text{Ca}^{2+}$  with or without 1.65 mM ADP stimulation driven by 5 mM succinate ( $n=4$ ). \* $P<0.05$  versus control; #  $P<0.05$ , ##  $P<0.01$  versus control with ADP. **(c)** Effect of 15 mM  $\text{HCO}_3^-$ , 25  $\mu\text{M}$  2HE and 5  $\mu\text{M}$  CsA on  $\Delta\Psi\text{m}$  loss induced by 10  $\mu\text{M}$   $\text{Ca}^{2+}$ . **(d)** Average half-time values of  $\Delta\Psi\text{m}$  loss induced by 10  $\mu\text{M}$   $\text{Ca}^{2+}$  calculated from panels **(c)** ( $n=7-20$ ). **(e)** Effect of 15 mM  $\text{HCO}_3^-$ , 25  $\mu\text{M}$  2HE and 5  $\mu\text{M}$  CsA on mitochondrial swelling induced by 10  $\mu\text{M}$   $\text{Ca}^{2+}$ . **(f)** Average half-time values of mitochondrial swelling induced by 10  $\mu\text{M}$   $\text{Ca}^{2+}$  calculated from panels **(e)** ( $n=7-20$ ). \*\* $P<0.01$ , \*\*\* $P<0.001$  versus control.

**Figure 5. Epac1 mediates cAMP effect on respiration and permeability transition.** **(a)** Western blot analysis of Epac1 and Epac2 isoforms in mitochondria (M), mitoplast (MP) and post mitoplast fraction (pMP). **(b)** Oxygen consumption measurement with the MitoXpress probe in the absence or presence of 15 mM  $\text{HCO}_3^-$ , 50  $\mu\text{M}$  CE3F4 and  $\text{HCO}_3^- + \text{CE3F4}$ . Control, untreated mitochondria, has been normalized to 100% ( $n=5$ ). **(c)** Effects of CE3F4 on  $\Delta\Psi\text{m}$  induced by 10  $\mu\text{M}$   $\text{Ca}^{2+}$ . **(d)** Average half-time values of  $\Delta\Psi\text{m}$  loss induced by 10  $\mu\text{M}$   $\text{Ca}^{2+}$  calculated from experiments such as shown in **(c)** ( $n=15$ ). **(e)** Effects of CE3F4 on mitochondrial swelling induced by 10  $\mu\text{M}$   $\text{Ca}^{2+}$ . **(f)** Average half-time values of mitochondrial swelling induced by 10  $\mu\text{M}$   $\text{Ca}^{2+}$  calculated from experiments such as shown in **(e)** ( $n=15$ ). \* $P<0.05$ , \*\* $P<0.01$ , \*\*\* $P<0.001$  versus control.

**Figure 6. Epac1 prevents  $\text{Ca}^{2+}$  entry into mitochondria via the  $\text{Ca}^{2+}$  uniporter and not the  $\text{Na}^+/\text{Ca}^{2+}$  exchanger.** **(a)** Measurement of  $\text{Ca}^{2+}$  accumulation in isolated mitochondria using Rhod-2.  $\text{HCO}_3^-$  was used at 15 mM, and CE3F4 was used at 50  $\mu\text{M}$ . **(b)** Half-time of  $\text{Ca}^{2+}$  entry into mitochondria calculated from experiments such as shown in **(a)** ( $n=5$ ). **(c)** Time course of  $\text{Ca}^{2+}$  accumulation in isolated mitochondria in the presence of 15 mM  $\text{HCO}_3^-$ , 50  $\mu\text{M}$  CE3F4 and 10  $\mu\text{M}$  CGP37157, a mNCX inhibitor. **(d)** Half-time of  $\text{Ca}^{2+}$  accumulation into mitochondria calculated from experiments such as shown in **(c)** ( $n=5$ ). **(e)** Time course of  $\text{Ca}^{2+}$  accumulation in isolated mitochondria in the presence of 15 mM  $\text{HCO}_3^-$ , 50  $\mu\text{M}$  CE3F4 and 0.4 nM Ru360 (MCU inhibitor). **(f)** Half-time of  $\text{Ca}^{2+}$  accumulation into mitochondria calculated from experiments such as shown in **(e)** ( $n=5$ ). \* $P<0.05$ , \*\* $P<0.01$ , \*\*\* $P<0.001$ .

**Figure 7. Epac1 mediates mitochondrial calcium accumulation and  $\Delta\Psi\text{m}$  loss in cellulo.** **(a)** Epac1 expression in neonatal rat cardiomyocytes transfected with non-targeting siRNA (si-Control) or Epac1 siRNA (si-Epac1). **(b)** Representative confocal images of TMRM-labeled permeabilized neonatal rat cardiomyocytes transfected with si-Control or si-Epac1 at time 0 s (left) and 900 s (right) after  $\text{Ca}^{2+}$  (600 nM) addition. Bar scale, 50  $\mu\text{m}$ . **(c)** Averaged values of  $\Delta\Psi\text{m}$  (measured as  $F/F_0$  where F is the TMRM fluorescence signal at 900 s and  $F_0$

is the signal at time 0 s of  $\text{Ca}^{2+}$  addition) (n=36). **(d)** Representative confocal images of Rhod-2 AM-labeled permeabilized neonatal rat cardiomyocytes transfected with si-Control or si-Epac1 at time 0 s (left) and 600 s (right) after  $\text{Ca}^{2+}$  (200 nM) addition. Bar scale, 50  $\mu\text{m}$ . **(e)** Averaged values of intra-mitochondrial  $\text{Ca}^{2+}$  accumulation (measured as F/F0 where F is the Rhod-2 fluorescence signal at 600 s and F0 is the signal at time 0 s of  $\text{Ca}^{2+}$  addition) (n=30). **(f)** Representative confocal images of Rhod-2 AM-labeled permeabilized adult rat ventricular myocytes at time 0 s (left) and 600 s (right) after  $\text{Ca}^{2+}$  (200 nM) addition in the absence (top) or presence (bottom) of CE3F4. Bar scale, 20  $\mu\text{m}$ . **(g)** Averaged values of intra-mitochondrial  $\text{Ca}^{2+}$  accumulation (measured as F/F0 where F is the Rhod-2 fluorescence signal at 600 s and F0 is the signal at time 0 s of  $\text{Ca}^{2+}$  addition) (n=10). \* $P$ <0.05 versus si-Control or Control.

**Figure 8. Expression levels of sACt, Epac1 and MCU in hearts and mitochondria isolated from Sham and HF rats and cAMP regulation of  $\Delta\Psi\text{m}$  and  $\text{Ca}^{2+}$  uptake.** **(a)** Expression level of sAC and Epac1 in Sham (white bars) and heart failure (HF, black bars) heart homogenates (H) normalized by GAPDH. Representative Western blot images are shown on top (Sham on left and HF on right). **(b)** Expression level of sAC<sub>t</sub>, Epac1 and MCU proteins relative to VDAC in isolated mitochondria (M) in HF versus Sham. Representative blots are shown on top (Sham on left and HF on right). Data are mean  $\pm$  SEM of 4 Sham and 4 HF rats, detected in four independent immunoblots. **(c)** Half-time of  $\Delta\Psi\text{m}$  loss induced by 10  $\mu\text{M}$   $\text{Ca}^{2+}$  calculated from experiments such as shown in Supplementary Figure 6a-b. **(d)** Half-time of  $\text{Ca}^{2+}$  accumulation calculated from experiments such as shown in Supplementary Figure 6c-d. **(e)** Half-time of swelling induced by 10  $\mu\text{M}$   $\text{Ca}^{2+}$  calculated from experiments such as shown in Supplementary Figure 6e-f. \* $P$ <0.05, \*\* $P$ <0.01, \*\*\* $P$ <0.001 versus Sham control; #  $P$ <0.05, ###  $P$ <0.001 versus HF control (n=4). **(f)** Hypothetical scheme showing the local role of mitochondrial cAMP signaling pathway. Within the mitochondrion, bicarbonate and calcium stimulate the production of cAMP by sAC<sub>t</sub>, which activates mitochondrial cAMP production. In turn, cAMP stimulates oxidative phosphorylation and inhibits permeability transition via activation of mitochondrial Epac1.

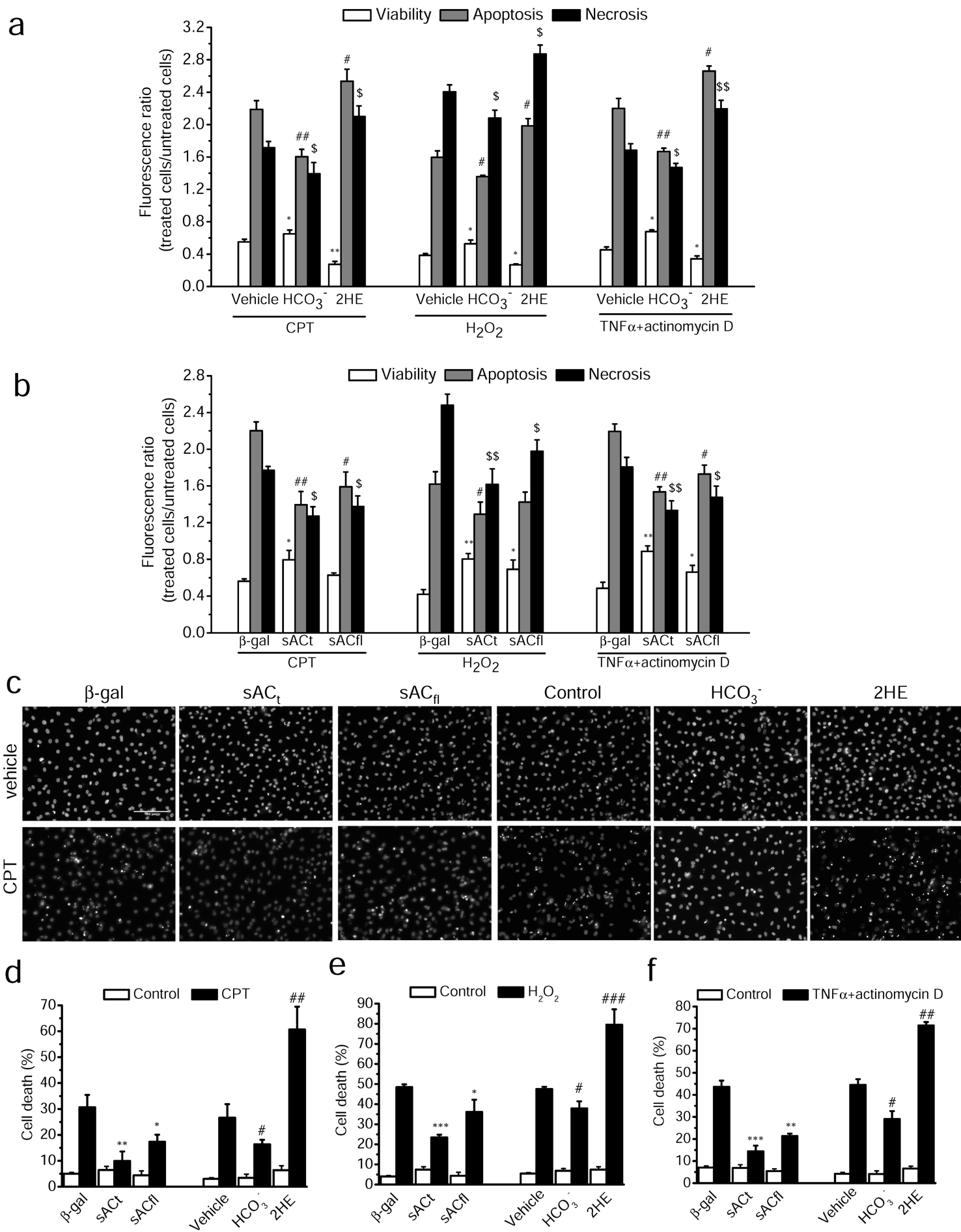


Figure 1

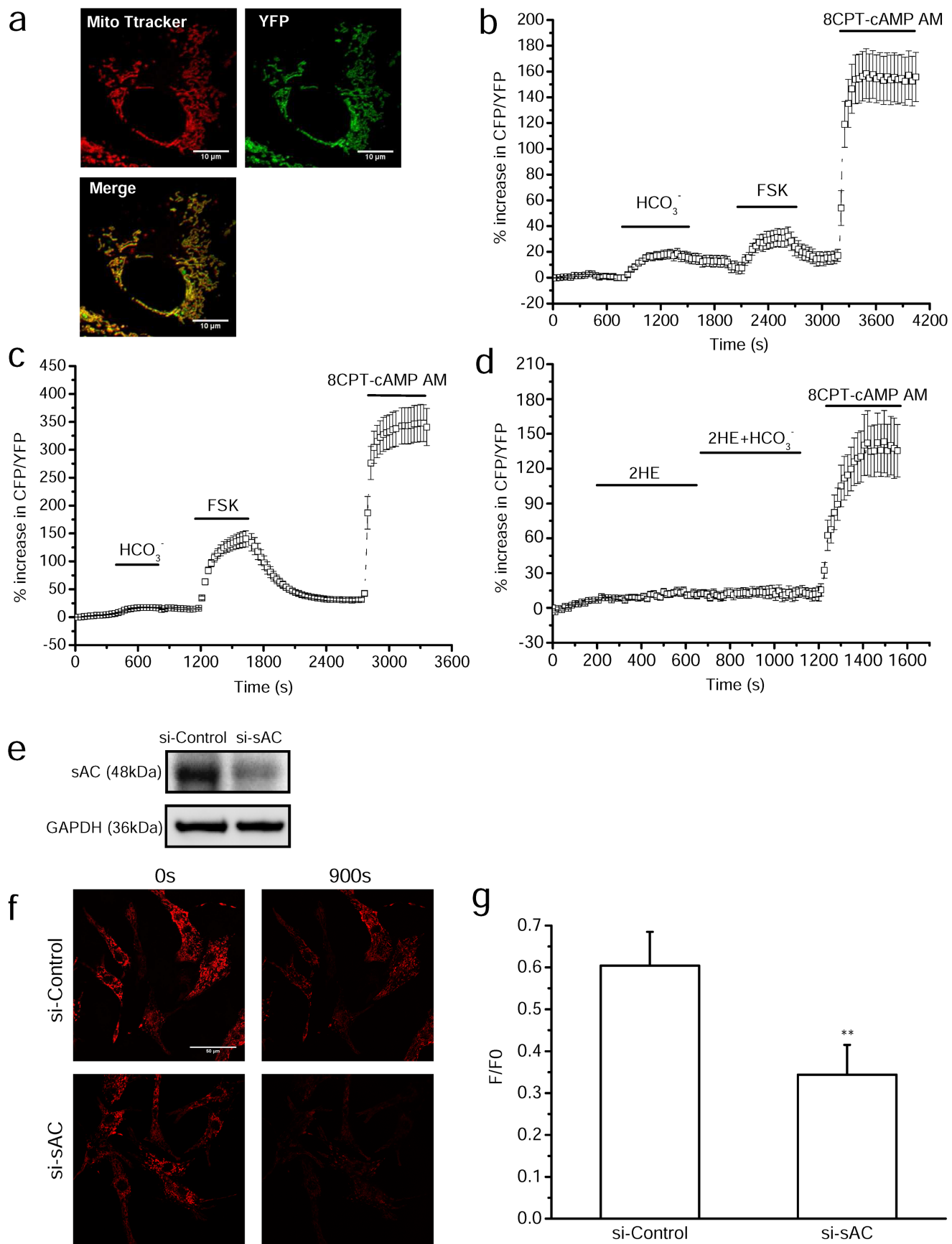


Figure 2

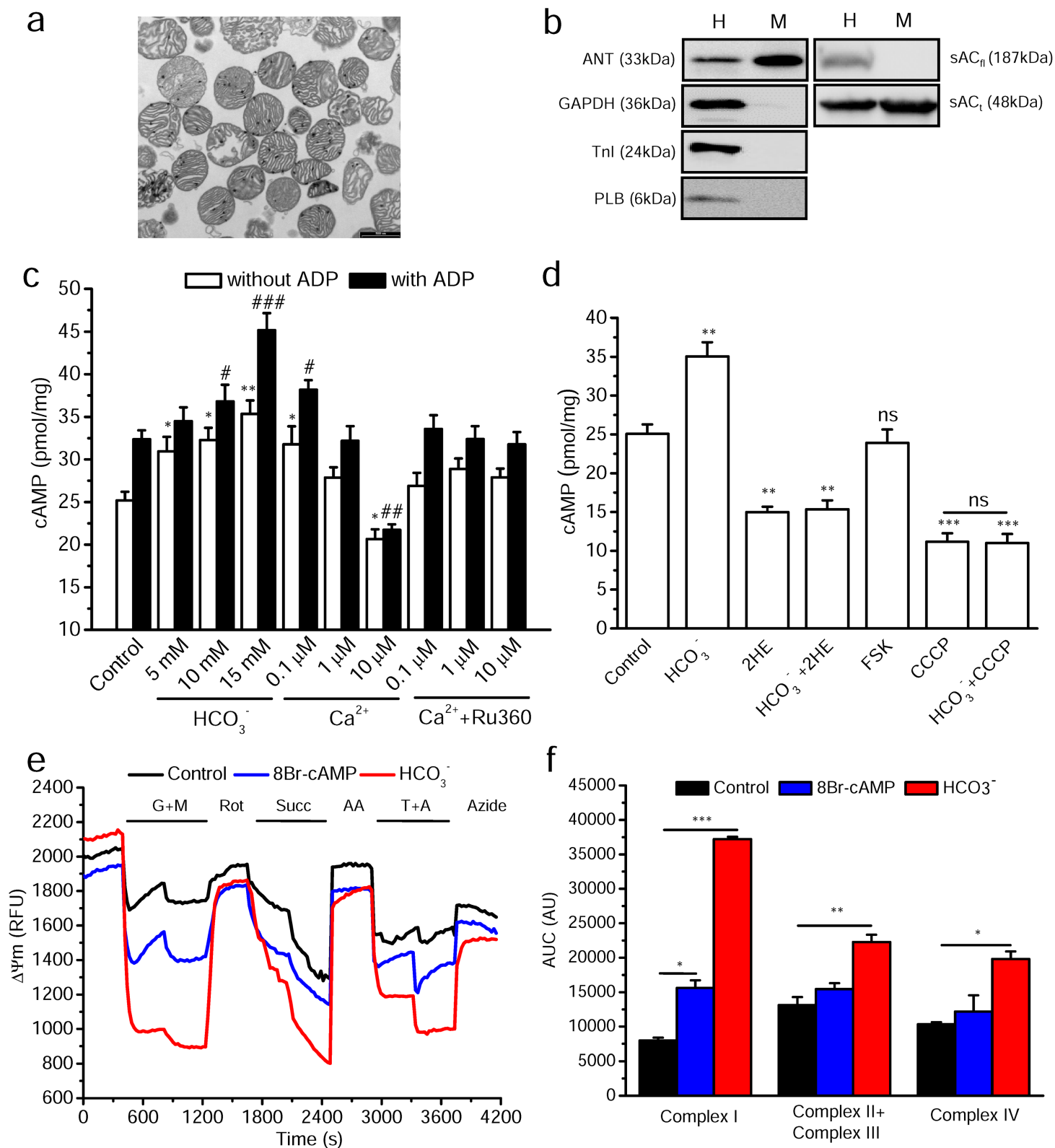


Figure 3

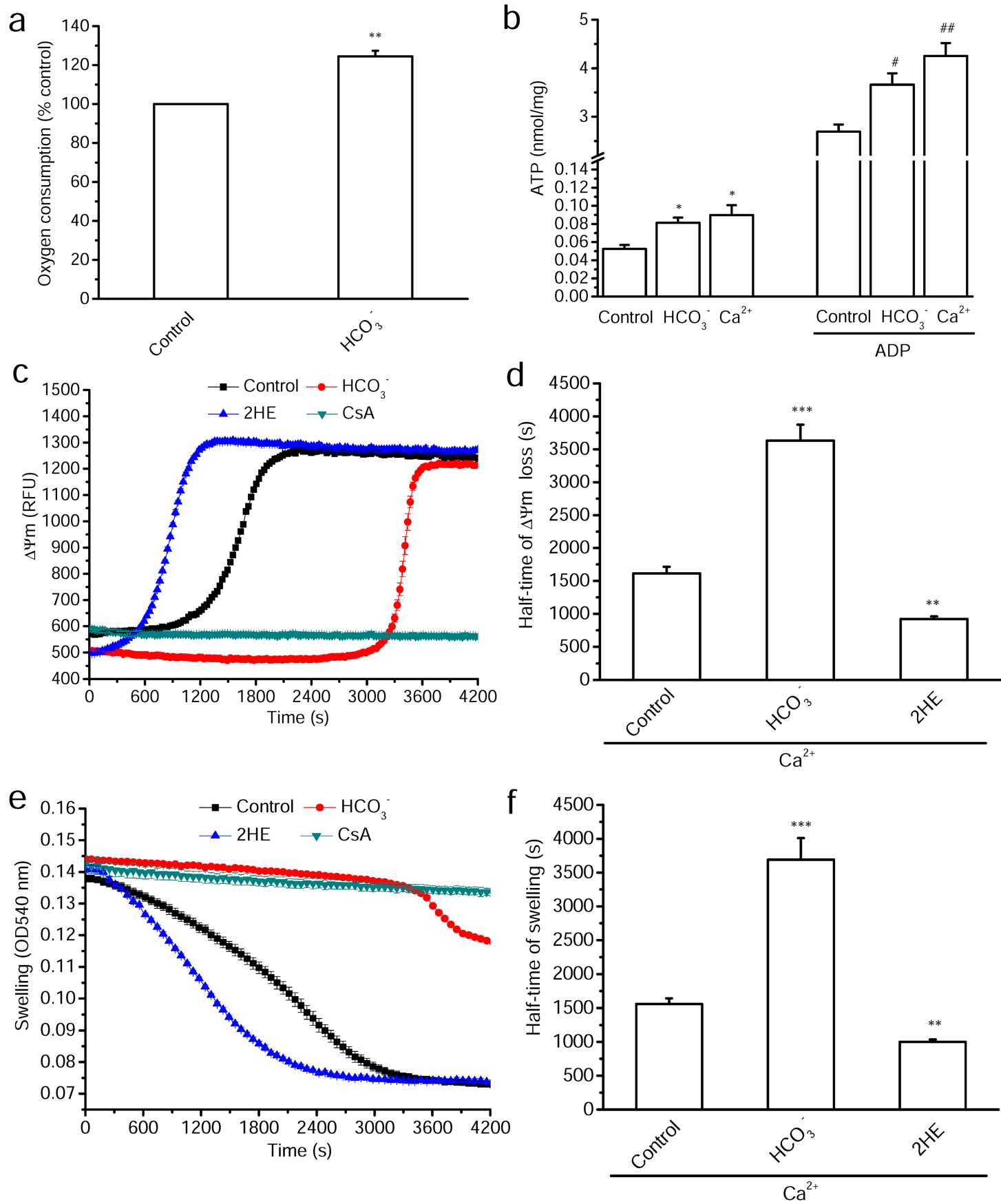


Figure 4

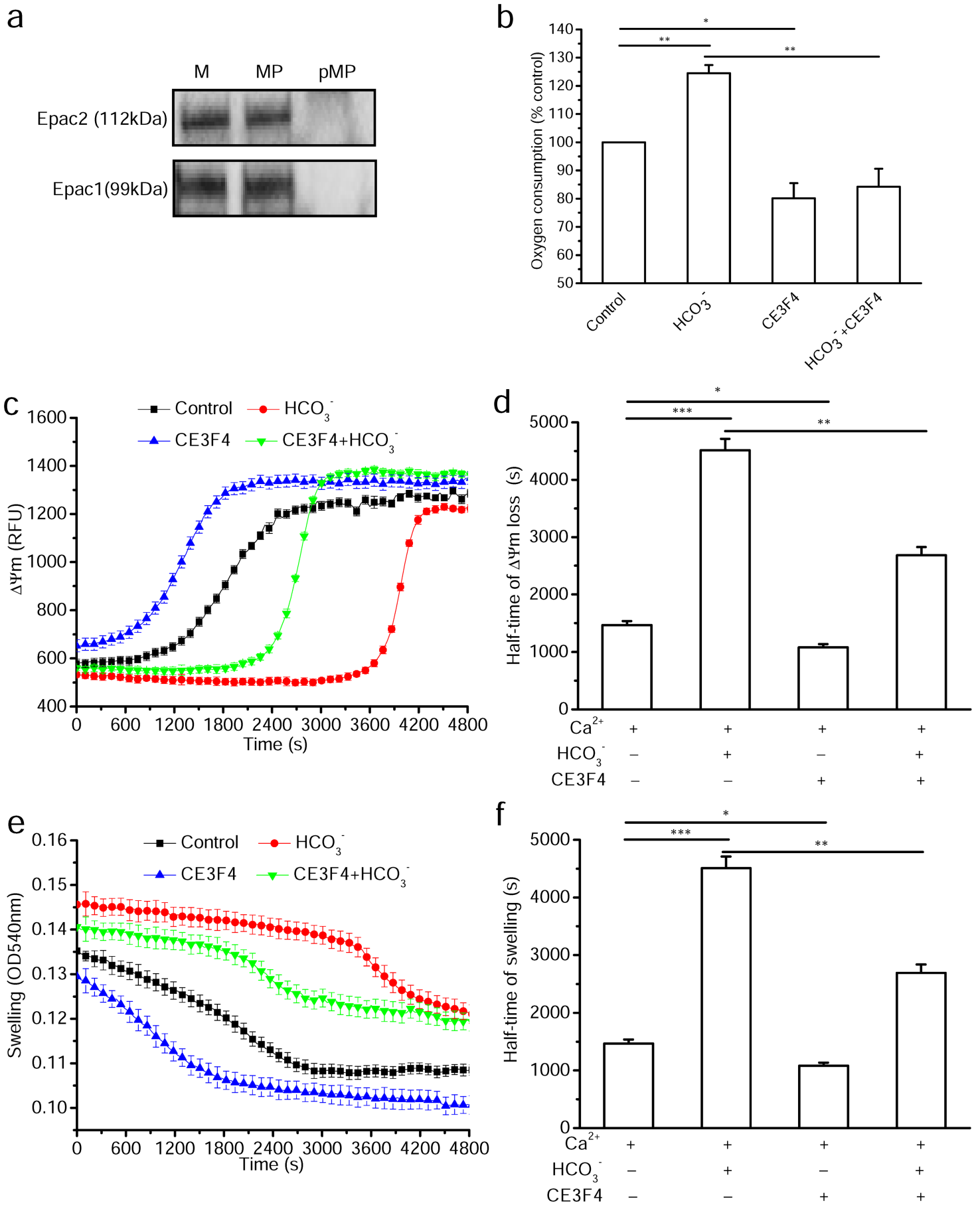


Figure 5

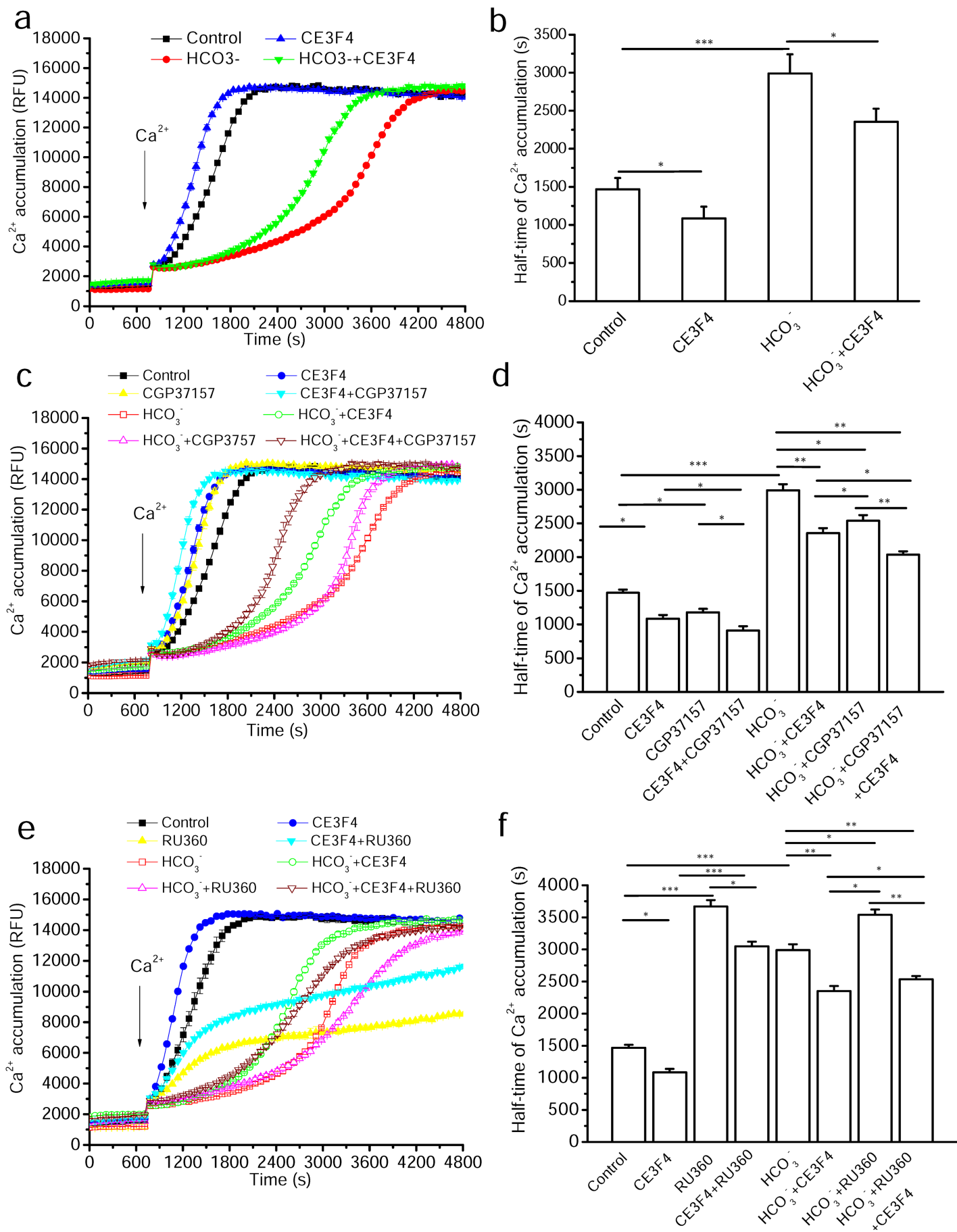


Figure 6

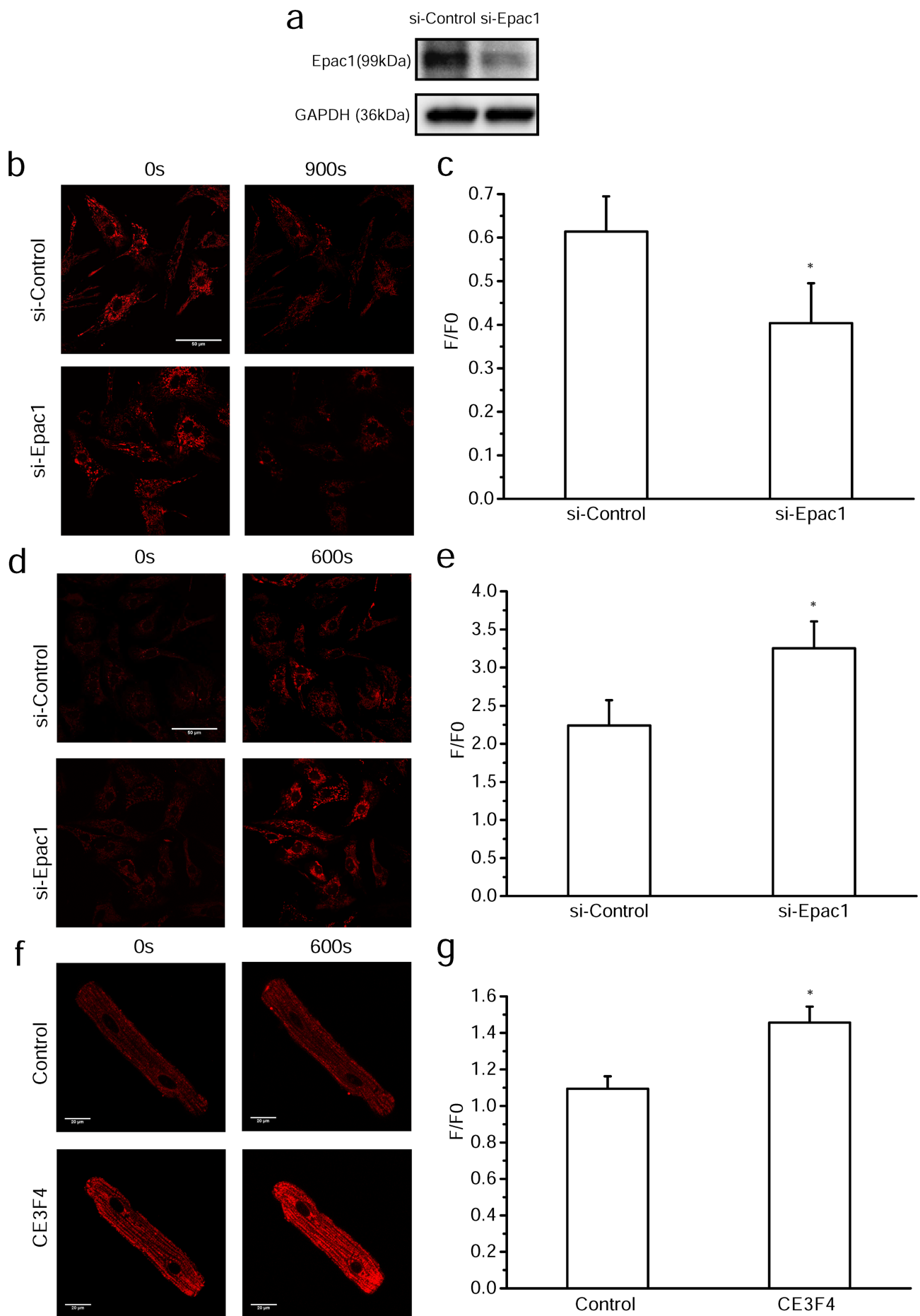


Figure 7

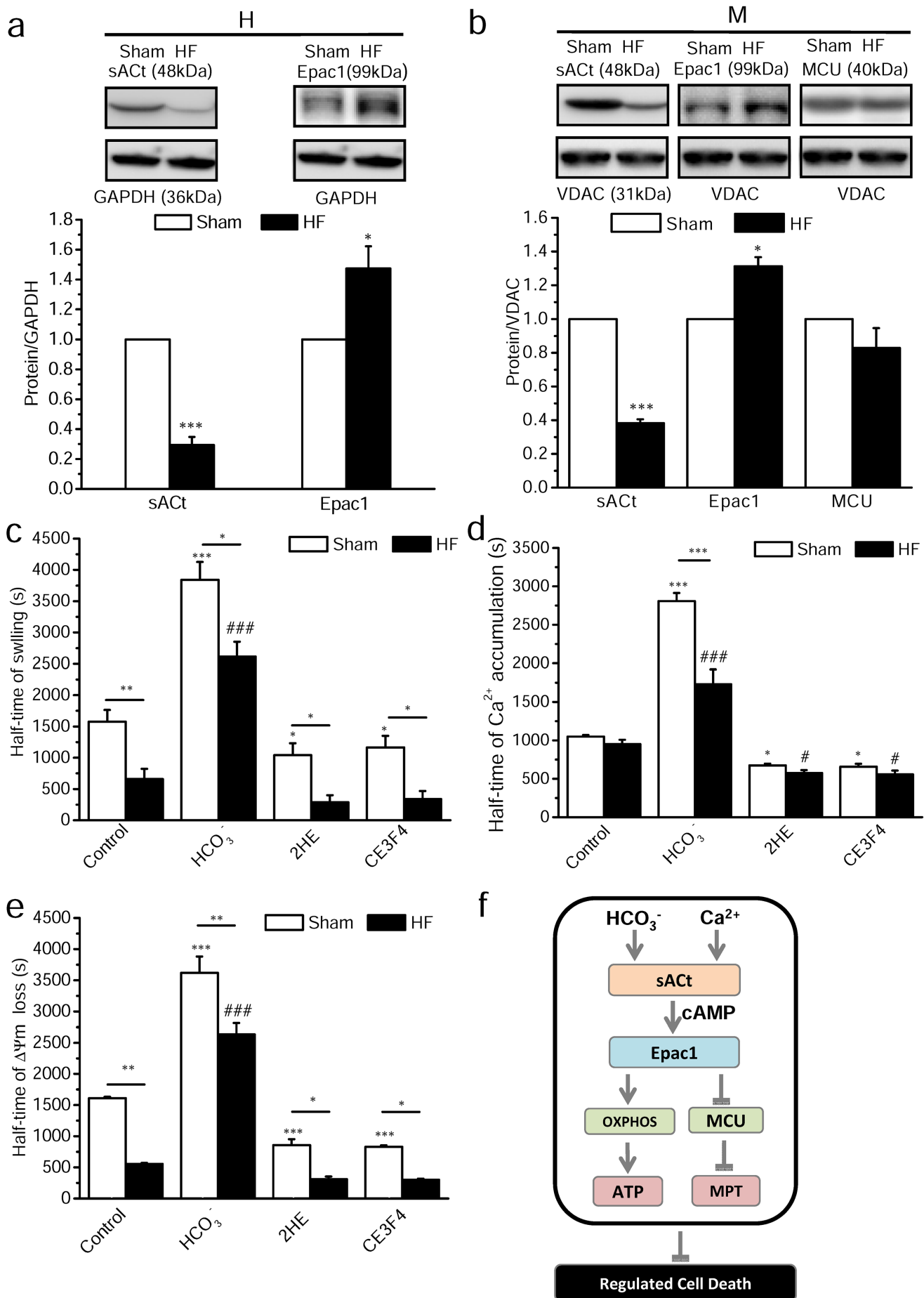


Figure 8